Handbook of Star Forming Regions Vol. II
Astronomical Society of the Pacific, © 2008
Bo Reipurth, ed.

Star Formation in NGC 6334

Paolo Persi

INAF-Istituto Astrofisica Spaziale e Fisica Cosmica Roma, Via Fosso del Cavaliere 100, 00133 Roma, Italy

Mauricio Tapia

Instituto de Astronomía, Universidad Nacional Autónoma de México, Ensenada, Apartado Postal 877, 22830 Ensenada, B.C., Mexico

Abstract. The bright nebula NGC 6334 extends nearly 0.4 square degrees across the sky and is located at a distance from the Sun of 1.61 kpc. This region contains some of the most active sites of massive star formation in our Galaxy. Discovered by their bright far-infrared emission associated with radio continuum peaks, these nuclei of activity are aligned along a dense molecular ridge that runs parallel to the Galactic Plane and stretches some 10 pc. It has a total mass of a few $10^5 M_\odot$. The physical characteristics of the active spots range widely, from well developed expanding HII regions to deeply embedded, still contracting, young objects detected only as millimeter sources, thus at their earliest observable stage of their evolution. The oldest optically visible round HII regions with central O-type stars are found in the southern parts. There is no clear spatial evolutionary correletion across the region. In this review we describe the observed characteristics of the giant molecular cloud complex and present detailed discussions on the individual centres of star formation.

1. The Giant Complex NGC 6334

This magnificent, if somewhat obscured, optical emission nebula, also known as the "Cat's Paw", is one of the most complex natural star formation laboratories known in the Galaxy. It extends $32' \times 40'$ across the sky, corresponding to 15×19 square parsec at a distance from the Sun of 1.61 kpc (Section 1.2) and is located less than 10° away from the Galactic Center ($l = 351^\circ$, $b = 0.7^\circ$). It comprises a giant molecular cloud where stars began forming several million years ago, and still continues to do so. The visible nebula, displayed in Fig. 1, is ionized by a small number of lightly reddened O-B0 stars which seem, in projection, to be scattered around the whole complex. The densest zones, including the projected centre of the nebulosity, are aligned parallel to the Galactic plane. Along this ridge, several well separated (typically some $2.5'$ or 2 pc) distinct active spots are located. Nevertheless, a few very young regions are at locations slightly off this "star forming" axis. Large-scale surveys made at different wavelength ranges have identified these very young spots and, because not all of them emit in all wavebands, several name sets have been proposed and this has contributed to some confusion. In particular, Roman numbers I to V were assigned to the far-infrared peaks by McBreen et al. (1979) and letters A to F to the radio sources by Rodríguez, Cantó & Moran (1982). The nomenclature adopted here is an extension of Kraemer and Jackson's (1999, Appendix) identification scheme.

Figure 1. A wide field image of the NGC 6334 region. The dark cloud near the upper left edge is Barnard 257. The field of view is approximately $90' \times 65'$. North is up, east is left. This is a composite Hα and broad-band image, courtesy of Martin Pugh.

Other composite multi-wavelength panoramic images of the whole region are shown in Figs. 2 to 5. Fig. 2 is a red DSS image with the O-B2 stars of the field indicated while the mid-infrared emission distribution is shown in Fig. 3. This is a composite from Midcourse Space Experiment *MSX* bands A, D and E (blue, green, red, respectively) images, covering the wavelength range 8.3 to 21.3 μm. The different active and past star formation sites are labeled and this identification scheme will be followed throughout this review. Fig. 4 shows a combined near-infrared *JHK* 2MASS mosaic. Fig. 5 illustrates a *Spitzer*/IRAC GLIMPSE survey mosaic in three wavelength bands: 3.6 μm (blue), 4.5 μm (green) and 8 μm (red). In this section, the global aspects of the the NGC 6334 complex in the different frequency regimes will be discussed, and Section 2 will provide detailed descriptions of each individual active spot.

1.1. The Optical Nebula

NGC 6334 is a very large, bright, optical nebula discovered in 1837 from the Cape of Good Hope by William Herschel, who catalogued it as H3678. It became GC 4288 in John Herschel's (1864) original *General Catalogue of Nebulae and Clusters of Stars*, which was the first such compilation, based mainly on his and his father's (William) observations. In the revised *New General Catalogue* (NGC) by Dreyer (1888), this emission nebula, NGC 6334, is described as "considerably faint, very large, of irregu-

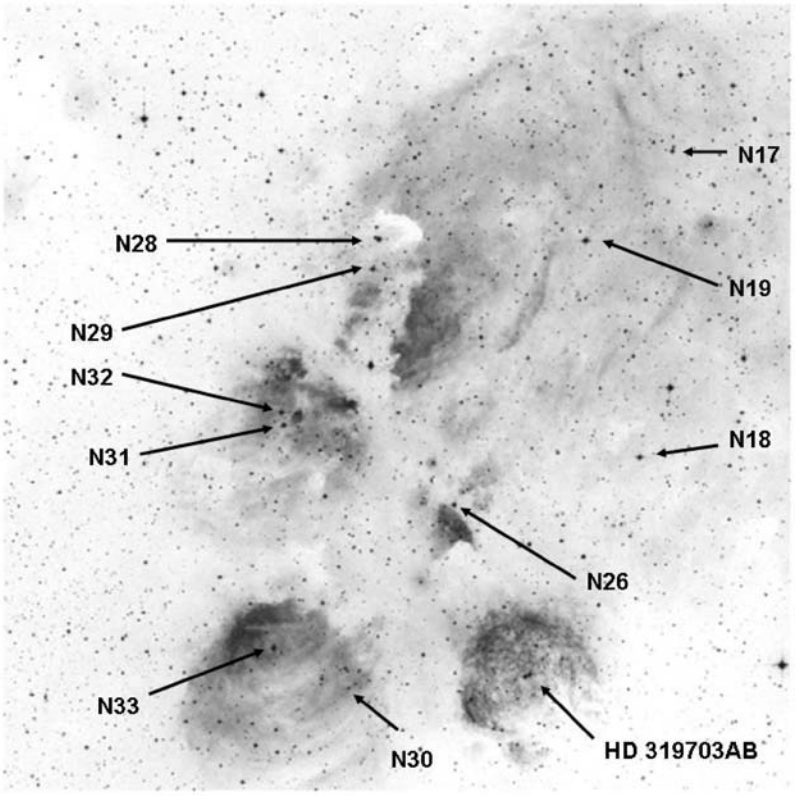

Figure 2. The red Digital Sky Survey image of the region centred at (J2000) $\alpha = 17^{\rm h}\ 20^{\rm m}\ 19.9^{\rm s}$, $\delta = -35^{o}\ 51'\ 24''$ containing NGC 6334 with the optically visible O-B2 stars marked as listed in Table 1.

lar figure, very gradually brightest towards the following (E) side". Early photographic surveys that included this nebula were by Sharpless (1953: No. 7: "composed of several detached portions"), Gum (1955: Nos. 61, 62, 63, 64), Hase & Shajn (1955: No. 119), Bok et al. (1955), Sharpless (1959: S 8) and Rodgers et al. (1960: RCW 127). Fig. 2 presents a photograph of the whole region ($42' \times 42'$) from the Digitized Sky Survey (DSS) in a red broad-band filter, with the strong nebular Hα emission dominating the emission. The O- to early B-type stars in the region are identified (see Table 1). The complexity of the region is evident from the variety of shapes and brightness of the several nebular components, clearly indicating large amounts of dust distributed in intricate ways. Several of the photographic surveys included identifications of a relatively small number of blue stars within the nebula as possible candidates for its ionization. The Hα radial velocity of NGC 6334 was measured by Georgelin & Georgelin (1970), who reported a value of $V_r = -11.4$ km s^{-1}, corresponding to $V_{LSR} = -3.6$ km s^{-1}.

When only optical images of the region were available (Figs. 1 and 2), one basic question remained unanswered: Are the several visible nebular components really independent substructures, maybe at different distances from the Sun, or is it one monolithic giant HII region where the distribution of absorbing dust makes it appear as a segmented nebula? The answer was not straightforward. Initially, it was determined that spectroscopic distance determinations to the putative ionizing optically-visible O-B0-type stars

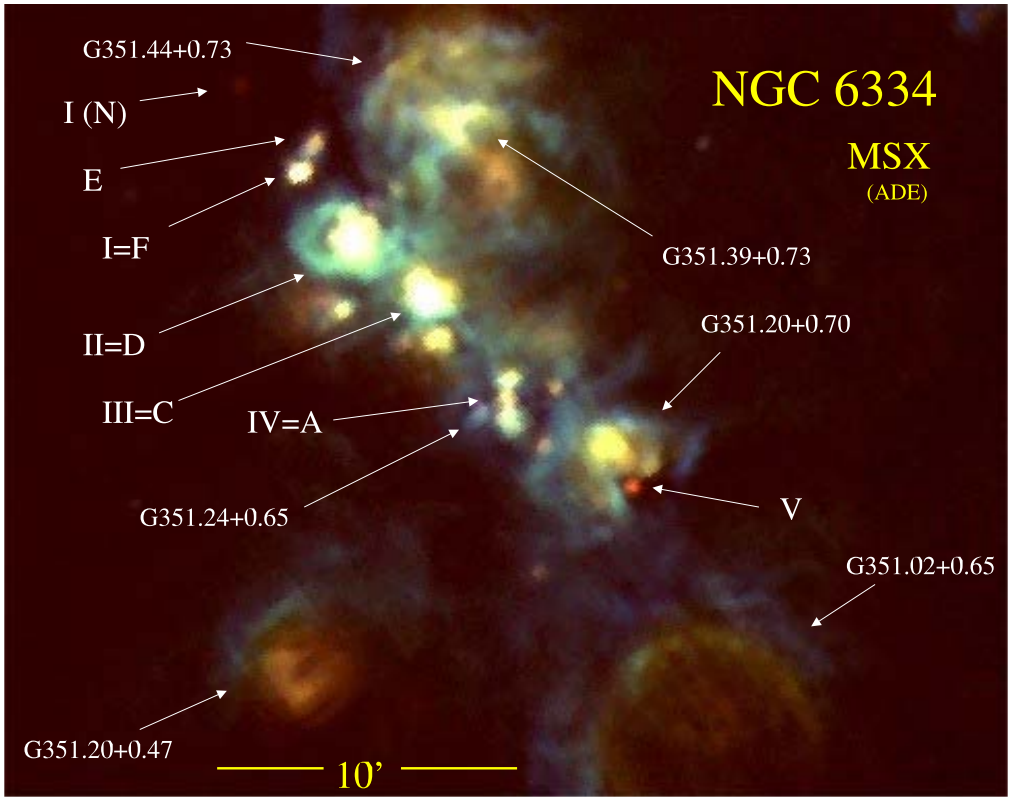

Figure 3. Colour-composite image of NGC 6334 in the mid-infrared. *MSX* band A (8.3 μm) image is in blue, band D (14.7 μm) in green and band E (21.3 μm) is in red. The radio HII regions and mid- and far-infrared sources are labeled according to the identification followed throughout the text.

yielded, within calibration errors, a single distance to all of them, suggesting that the whole NGC 6334 nebula is a single, large and complex system. It later became clear that this unified concept is also supported by available large-scale multiwavelength observations.

As will be described in the following sections, there is now clear evidence that what we are witnessing today is the result of the evolution of an originally single giant molecular cloud that, once the first localized event of star formation occurred, triggered subsequent and un-orderly similar events within the cloud. At present, the region is believed to form a very complex collection of active spots, each with its own energetics and history. Unfortunately, the line-of sight structure of this complex is completely unknown, and without this indispensable piece of information, it will be impossible to understand the physics of this sequence of star-forming events.

It is curious that as of today, no large-scale detailed spectroscopic study of the optical nebula is available in the literature. Gyulbudaghian, Glushkov & Denisyuk (1978), based on examination of the Palomar Survey plates, reported a suspected single Herbig-Haro object (GGD 25) in the vicinity of a very young far-infrared and radio source (IV = A) near the centre of NGC 6334. Bohigas (1992) proved that this small nebulosity is photoionized and, thus, it is just a small component of the huge HII region.

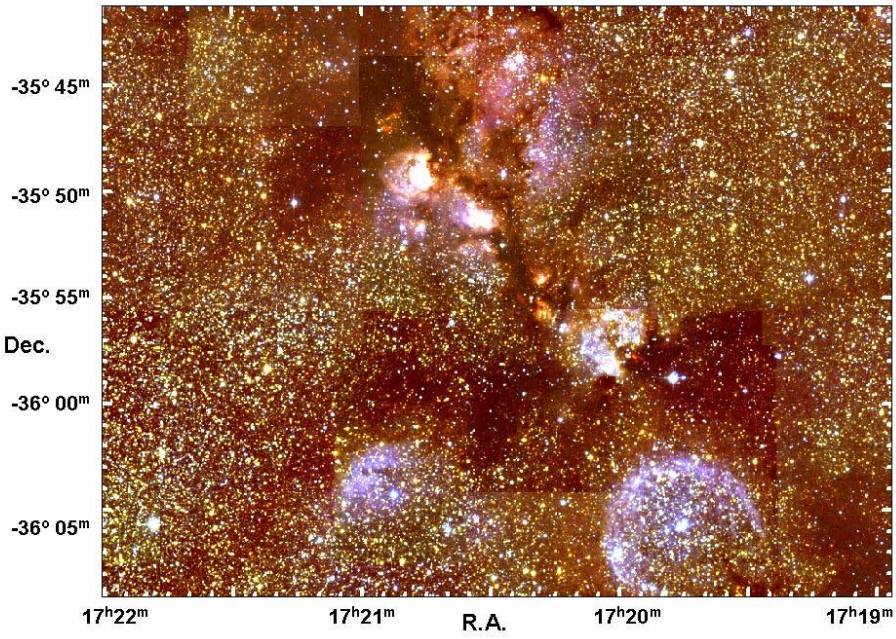

Figure 4. 2MASS *JHK* colour-composite image of NGC 6334.

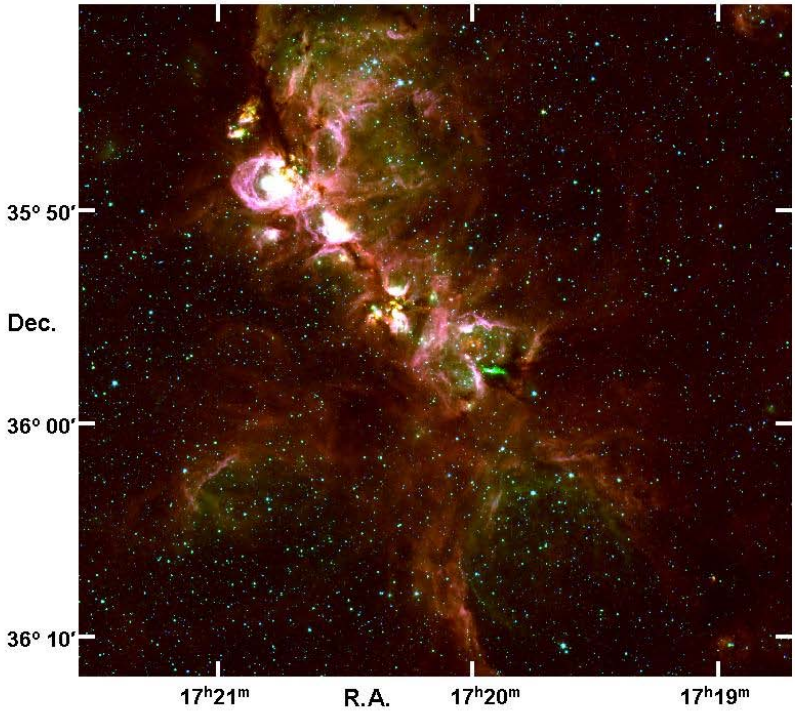

Figure 5. *Spitzer*/IRAC colour-composite image of NGC 6334 from the GLIMPSE survey. IRAC channel 1 (3.6 μm) image is in blue, channel 2 (4.5 μm) in green and channel 4 (8 μm) is in red. The coordinates are J2000.

1.2. Distance

A small number of visible very luminous blue stars, indicated in Fig. 2, have been identified within NGC 6334. Accurate photometry of these have been reported by Neckel (1978) and by Walborn (1982), who also provided two-dimensional spectral classification of five O-type stars in the complex. Table 1 summarizes the available stellar data for early-type stars in the region providing the ionizing energy to the visible HII regions. Spectroscopic distance determinations based on these data are certainly the most accurate and reliable, particularly because kinematic distance determinations in the direction of NGC 6334, which is very close to the Galactic Center ($l \sim 353^{\circ}$), are extremely uncertain. Roslund (1966), Neckel (1978) and Walborn (1982) have computed distances to the visible early-type stars in the region, obtaining $d = 1.45$ kpc, 1.74 kpc and 2.30 kpc, respectively. The discrepancies, though not too large, are due to the different M_V calibrations adopted by each author. A different sort of inaccuracy in these determinations was caused by their assumed "normal" extinction law ($R_V = 3.0 - 3.1$). Using Neckel's (1978) photometry, Neckel & Chini (1981) found later that the value of the total to selective extinction ratio $R_V = A_V/E(B-V)$ for NGC 6334 was close to 4, characteristic of many other Galactic star forming regions.

We have determined new values of A_V and $V_o - M_V$ for the stars in Table 1, using more reliable absolute-magnitude calibrations and, more importantly, have based the computation of A_V on the colour excess index transformation $A_V = 1.39E(V - J)$, which is constant across the Galaxy, irrespective of high R_V values (Tapia et al. 1988). For the eleven OB stars ionizing the optical HII nebulae in NGC 6334, we obtain $< A_V >= 4.12 \pm 0.20$ and $< V_o - M_V >= 11.03 \pm 0.10$ which corresponds to $< d >= 1.61 \pm 0.08$ kpc. Thus, $1'$ corresponds to 0.47 pc. It is important to note that most previous multi-wavelength studies of this complex have assumed Neckel's (1978) value (1.7 or 1.74 kpc) for the distance to NGC 6334, which is about 6 to 8% higher than the one presented here, meaning that the derived physical quantities that scale as d^2 have been overestimated by only 11 to 17%.

1.3. Distribution of the Ionized Gas: Radio Continuum Maps

NGC 6334 was catalogued as a thermal-spectrum radio source by Wilson & Bolton (1960) (CTB 39) and the whole HII region was mapped in the radio continuum at $\lambda = 6$ cm (5000 MHz) with the Parkes 210 foot antenna by Goss & Shaver (1970) with a $4'$ beam. Schraml & Mezger (1969) obtained maps of the central region with a $2'$ beam in the H109α line ($V_{LSR} = -2.5$ km s^{-1}) and in the 1.95 cm continuum. Note that the latter work contains an error in the coordinates of their NGC 6334 maps and corresponding entry in their Table 3 that amounts to $\Delta\alpha = 42''$, $\Delta\delta = 93''$ (Gardner & Whiteoak 1975, McBreen et al. 1979). A composite plot of both contour maps is shown in Fig. 6 displayed over the red Digital Sky Survey image where the extended emission is dominated by the Hα line. It is interesting to note that the outlying contours of the radio continuum maps align almost perfectly with the area covered by the Hα emission, implying that the ionized gas away from the dense molecular ridge is very lightly reddened. Indeed, the discrepancies are in the peak emission regions on the dense "activity ridge", where the radio peaks lie on highly obscured areas. The whole active ridge of star formation was mapped with high spatial resolution at 6 cm using the small radio sources (labeled A to F), one of which (B) was found later to be an extragalactic source (Moran et al. 1990) and therefore ignored in this review. The remaining five sources are HII regions associated with the molecular cloud displaying

Table 1. Coordinates, magnitudes, spectral types and distance moduli of OB stars

ID	A.R. (J2000) h m s	Dec. ° ′ ″	V	$B-V$	$U-B$	K	$J-H$	$H-K$	Sp. Ty.	A_V	V_o-M_V	Other ID
CD-35 11146	17 19 07.5	-35 37 46	11.44	0.76	-0.04	9.36	0.24	0.09	B2 IV	3.28	10.96	N17
HD 319701	17 19 16.0	-35 54 08	10.10	1.08	0.04	6.83	0.37	0.21	B1 Ib	4.73	11.57	N18
HD 319699	17 19 30.4	-35 42 36	9.63	0.77	-0.24	7.30	0.22	0.15	O5 V ((f))	3.74	10.89	N19
CD-35 11477	17 20 05.0	-35 56 38	11.11	0.90	-0.03	8.61	0.27	0.09	B1 V	3.82	10.79	N26
HD 319698	17 20 11.9	-35 43 42	10.79	0.26	-0.04	8.95	0.16	0.12	A0 II	-	-	N27
HD 319697	17 20 24.8	-35 42 32	10.33	0.66	-0.24	8.67	0.18	0.04	B1 V	2.84	10.99	N28
CD-35 11482	17 20 26.5	-35 44 07	10.70	0.73	-0.25	7.26	0.38	0.43	B0.5 Ve	-	-	N29
CD-35 11483	17 20 33.6	-36 06 26	11.65	1.03	-0.10	8.64	0.30	0.19	B1e	4.35	10.80	N30
HD 319703B	17 19 45.0	-36 05 47	11.2	1.25	0.04	7.59:	0.28:	0.28:	O6.5 V((f))	5.25	10.95	
HD 319703A	17 19 46.2	-36 05 52	10.71	1.14	0.04	7.03	0.38	0.27	O7.5 III((f))	4.88	11.43	
CD-35 11484	17 20 49.8	-35 52 21	11.33	0.95	0.04	8.57	0.27	0.18	B1 V	4.21	10.48	N31
HD 319702	17 20 50.6	-35 51 46	10.13	0.90	0.04	7.39	0.31	0.17	O8 III((f))	4.18	11.47	N32
HD 156738	17 20 52.7	-36 04 21	9.37	0.86	-0.14	6.76	0.26	0.16	O6.5 III(f)	4.09	10.98	N33

Identifications from (N) Neckel (1978). *JHK* photometry from 2MASS.
Optical data from Walborn (1982) for O-stars, Neckel (1978) for B-stars.
$A_V = 1.39E(V-J)$, M_V from Conti (1988), $(V-J)_o$ from Johnson (1966)

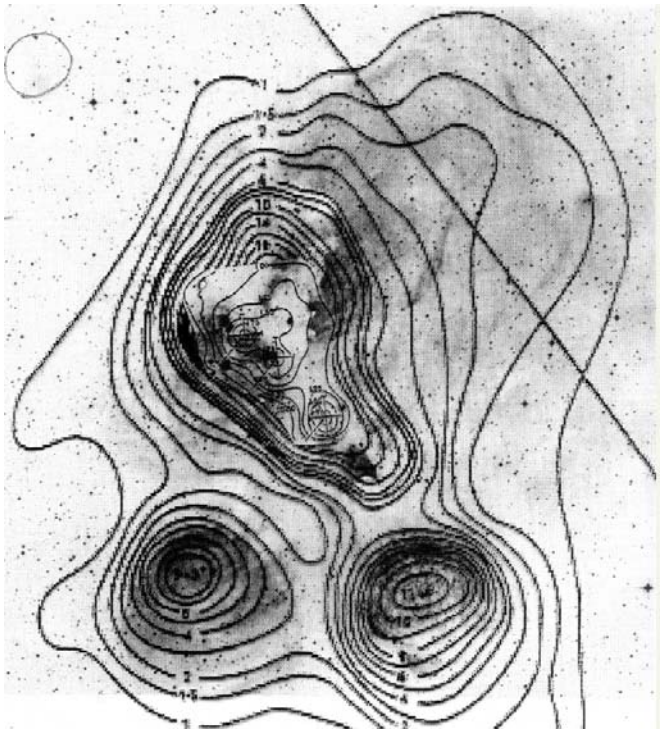

Figure 6. A composite contour plot of the radio continuum emission of NGC 6334. The thick, labeled contours are from the 6 cm survey by Goss & Shaver (1970) and the thin contours in the brightest region are from Schraml & Mezger's (1969) 1.95 cm survey. The crosses mark the position of the far-infrared peaks (see Section 1.4). The diagonal thick straight line goes parallel to the galactic equator with $b = 0.9^{\circ}$ The gray-scale image is from the red Digital Sky Survey. The field of view is $38' \times 45'$.

a wide range of sizes, from very compact (e.g. A and F) and presumably very young, to extended ($> 40''$) and well developed (e.g. E). There are also round, extended radio and bright optical HII regions at the southern edge, G351.20+0.47 and G351.02+0.65, first reported in the radio by Goss & Shaver (1970). Rodríguez, Cantó and Moran (1982) concluded that the observed shapes of the radio sources on the molecular ridge could be explained in terms of hydrodynamical models of the evolution of HII regions.

Sarma et al. (2000) mapped the whole region at 18 and 21 cm and obtained OH and H I absorption profiles. Their continuum observations cover the whole area and provide a comprehensive overview of the ionized gas with a $16'' \times 12''$ resolution. Figs. 7 and 8 show the 18 cm continuum emission contours displayed over the 2MASS/*JHK* and *MSX*/ACE mosaics of the central $18' \times 18'$ of the complex. We emphasize that all mid-infrared emission features seen on *MSX* maps are also detected in the radio continuum, including the diffuse emission extension to the NW of NGC 6334 II and the small, fainter components close to FIR sources II, III and IV. In fact, as expected, these higher resolution and more sensitive maps are consistent with the released 21 cm image from the NRAO/VLA Sky Survey (NVSS, Condon et al. 1998) and with a similar 18 cm continuum map by Brooks & Whiteoak (2001) made with ATCA while surveying the area for OH masers. Only the NVSS unresolved compact HII regions G351.44+0.73

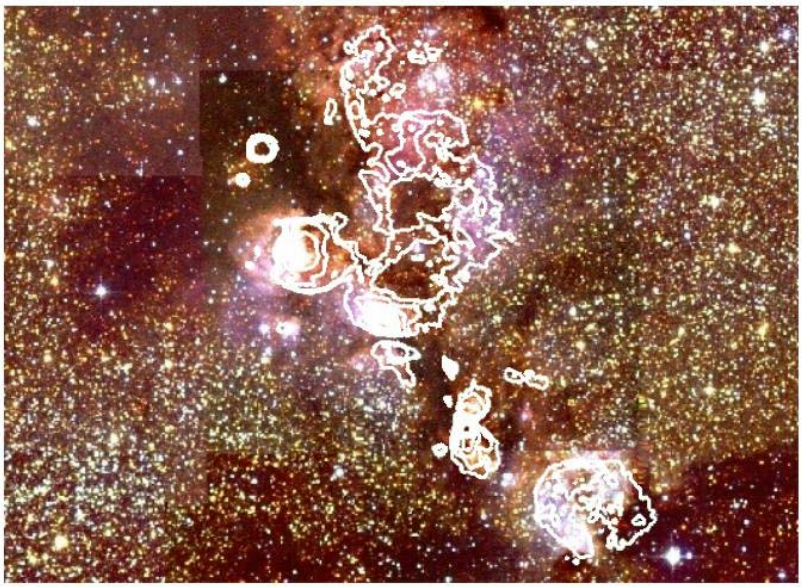

Figure 7. Contour map of the 18 cm continuum emission by Sarma et al. (2000) over a composite 2MASS *JHK* image. The field size is $24.5' \times 17.5'$ and is centred at $\alpha = 17^{\rm h}\ 20^{\rm m}\ 31.0^{\rm s}$, $\delta = -35^{o}\ 51'\ 09''$.

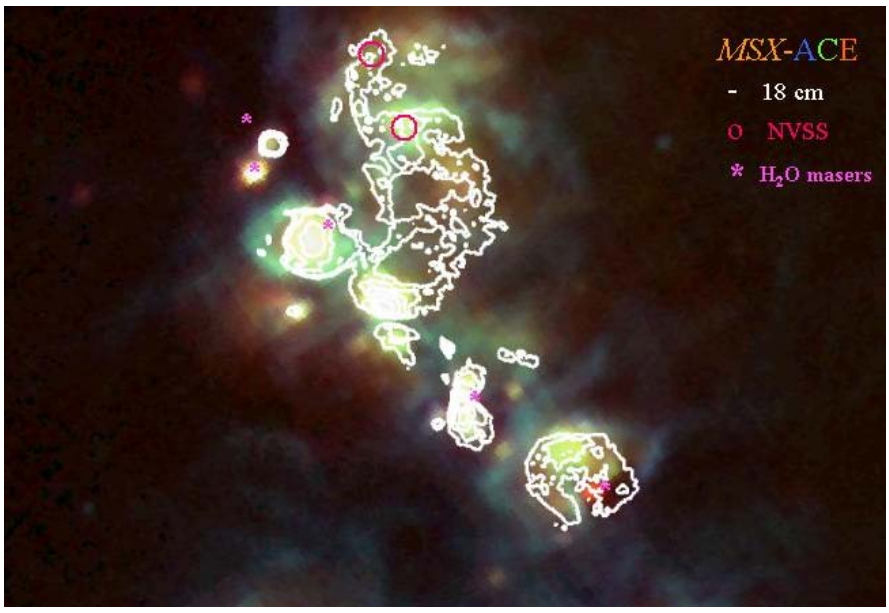

Figure 8. Contour map of the 18 cm continuum emission by Sarma et al. (2000) over the colour-composite of *MSX* images in the A (8.3 μm), C (12.1 μm) and E (21.3 μm) bands centred at $\alpha = 17^{\rm h}\ 20^{\rm m}\ 20.0^{\rm s}$, $\delta = -35^{o}\ 52'\ 00''$. The northern compact HII regions located from the NRAO/VLA Sky Survey (NVSS) image and the H_2O maser sources (Moran & Rodríguez 1980) are marked. The scale is the same as in Fig. 7.

and G351.39+0.73 are seen embedded in the more diffuse extended emission evident in Sarma et al.'s map. Sarma et al. (2000) also measured Zeeman splitting in the H I and OH lines in the direction of sources A, D and E, indicating magnetic field values of the order of 200 μG in these spots.

1.4. Distribution of the Molecular Gas: Molecular Line Maps

The first molecular gas emission maps of the region in the ^{12}CO, ^{13}CO lines ($J = 1 - 0$) were performed by Dickel, Dickel & Wilson (1977) from Kitt Peak National Observatory with a spatial resolution of around 70″. Even with such low resolution, they were able to discern four distinct emission peaks or "centres of activity" which correspond to the far-infrared sources V, IV, I and a point midway between II and III (Section 2). Dickel et al. could explain the observed morphology and line velocities with a simple model of a giant cloud collapsing with a $v \propto r^{\alpha}$ law and the several star formation sites embedded at different depths. Higher resolution maps in several transitions of ^{12}CO, ^{13}CO, CS and NH_3 by Jackson & Kraemer (1999) show that the molecular gas has a complex filamentary structure along the dense molecular ridge. Fig. 9 shows the ^{12}CO $J = 2 - 1$ emission map, which is similar to that of ^{13}CO, combined with a synthesized map in the 21 cm radio continuum emission from NVSS. These maps agree with Dickel et al.'s findings that the spots of star formation activity, as signposted by far-infrared maxima, are coincident with molecular line emission peaks. Recently, the complex has been mapped in the ^{12}CO $J = 4 \rightarrow 3$ rotational transition and in the ^{12}[CI] $^3P_2 \rightarrow ^3P_1$ fine-structure line by Kim & Narayan (2006). The details of the characteristics of the molecular gas in the individual regions, as observed also in other molecules, will be described in detail in Section 3.

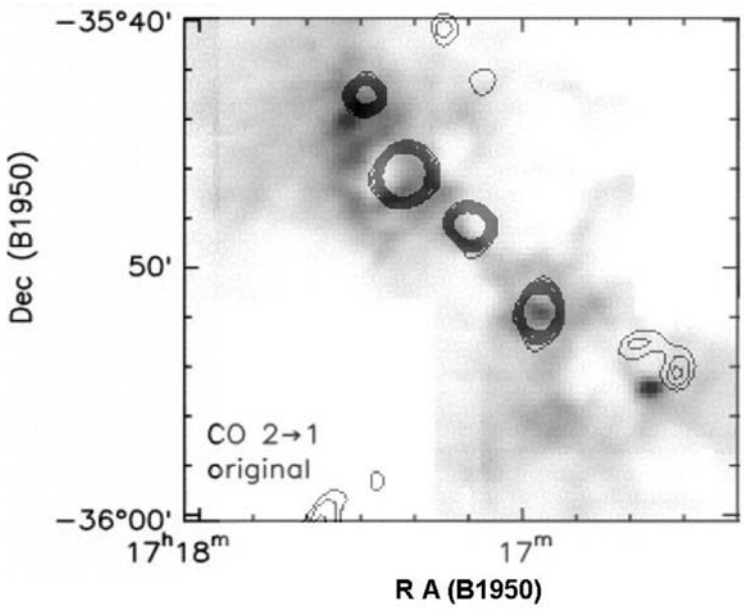

Figure 9. Kraemer & Jackson's (1999) ^{12}CO $J = 2-1$ integrated intensity map in grey scale (increasingly, white to black) with contours from the 21 cm NRAO/VLA Sky Survey (NVSS).

By adopting a single-component non-LTE excitation model, Kraemer & Jackson (1999) determined the following mean values for the average kinetic temperature T_k, molecular hydrogen column density $n_{\rm H_2}$, and volume density $N_{\rm H_2}$: $< T_k >= 56 \pm 11$ K, $< N_{\rm H_2} >= 7 \pm 4 \times 10^{22}$ cm^{-2}, and $< \log n_{\rm H_2} >= 3.5 \pm 0.3$ cm^{-3}. The densest spots are located to the southwest, in regions IV (= A) and V. CO and CS radial velocities peak in the centre of the ridge with lower (more negative) values observed at the edges (regions I and V) where the "ridge" becomes much wider. As pointed out by Jackson & Kraemer (1999), it is interesting to note the presence of regions that lack CO emission or "bubbles" close to dense emission peaks, these being somewhat correlated with Hα and [CII] emission, possibly implying that at least some of the CO emission minima, or "molecular holes", contain photodissociated gas. This conclusion was based on the work by Kraemer et al. (2000), who mapped the region in the fine-structure transitions of [CII] 158 μm and [OI] 63 and 146 μm with the Far-Infrared Fabry-Perot Interferometer on board the Kuiper Airborne Observatory (see also Boreiko & Betz 1995 and Kraemer et al. 1998).

2. Infrared and Millimeter Surveys

A good number of infrared and millimeter surveys of the entire dense molecular ridge have been made in the last thirty years and these are summarized in Table 2.

2.1. Far-infrared and Millimeter Maps

As part of a pioneering balloon-borne telescope survey of Galactic HII regions, Emerson et al. (1973) obtained a low resolution map of the whole region in a single, very broad, 40-350 μm bandpass. They found an emission structure that followed quite closely the one found in the radio continuum. They reported three far-infrared peaks which appeared to be related to the compact radio HII regions, but positional uncertainties in both radio and infrared maps made the comparison quite unreliable. In fact, the low spatial resolution may have caused that two pairs of active spots were unresolved in this map. During a similar far-infrared balloon-borne survey with improved resolution, McBreen et al. (1979) were able to resolve five far-infrared sources (designated I to V) approximately equally spaced along the molecular ridge with a large and diffuse emission in the northeastern region. Loughran et al. (1986) used the same balloon-borne telescope to map simultaneously the same area in four wavebands ($\lambda_{\rm eff}$ = 21, 42, 71 and 134 μm) with $\Delta\lambda/\lambda$ between 0.1 to 0.3. These authors could discern seven compact far-infrared sources, confirming those already discovered (I to V) and adding the extremely cold source, designated I(N) by Cheung et al. (1978) and Gezari (1982), that was undetected at $\lambda < 100\,\mu$m. They also resolved a source that coincided with the developed radio HII region E (Rodríguez et al. 1982). From the distribution of the dust temperature in the large ($> 8'$) lobe of far-infrared emission to the northwest of source I, Loughran et al. (1986) concluded that the heating ought to be caused by internal sources and not by sources on the molecular ridge. In fact, two compact HII regions (G351.44+0.73 and G351.39+0.73) are located within this lobe. The total luminosity of the eight sources was determined to be 1.7×10^6L$_\odot$and a total mass of 1.4×10^5M$_\odot$. Finally, Loughran et al. (1986) proposed that a Rayleigh-Jeans instability created by acceleration toward the Galactic Plane may explain the regular separation of the centres of activity in the cloud.

Table 2. Summary of infrared and millimeter surveys of the entire NGC 6334 molecular ridge

Wavelength (μm)	Date	telescope	FWHM	Reference
1200	2002-3	SEST 15m dish	$24''$	Miettinen et al. (2006), Muñoz et al. (2007)
40 - 350	1972	UCL 40 cm balloon	$3.5'$	Emerson et al. (1973)
40 - 250	1975	CfA/UAz 102 cm balloon	$1.3'$	McBreen et al. (1979)
21, 42, 71 and 134	1979	CfA/UAz 102 cm balloon	$1.0'$	Loughram et al. (1986)
12, 25, 60 and 100	1983	*IRAS* 57 cm satellite	$4'$	*Infrared Astronomical Satellite*
8.3, 12.1, 14.7 and 21.3	1996	*MSX* 33 cm satellite	$20''$	*Midcourse Space Experiment*
2.4, 3.3, 3.5 and 4.05	1998	South pole 60 cm tel.	$25''$	Burton et al. (2000)
3.6, 4.5. 5.8 and 8	2005	*Spitzer* 85 cm satellite	$2''$	GLIMPSE; Benjamin et al. (2003)
JHK ($K \lesssim 11$)	1984-85	MSO 1.8 m tel.	$3''$	Straw & Hyland (1989)
JHK ($K \lesssim 14$)	1983-87	AAT 3.9 m tel.	$2''$	Straw et al. (1989)
JHK ($K \lesssim 14$)	1999	CTIO 1.3 m tel.	$2''$	2MASS; Skrutskie et al. (2006)
JK ($K \lesssim 16$)	2002	LCO 2.5 m tel.	$1''$	In preparation (these authors)

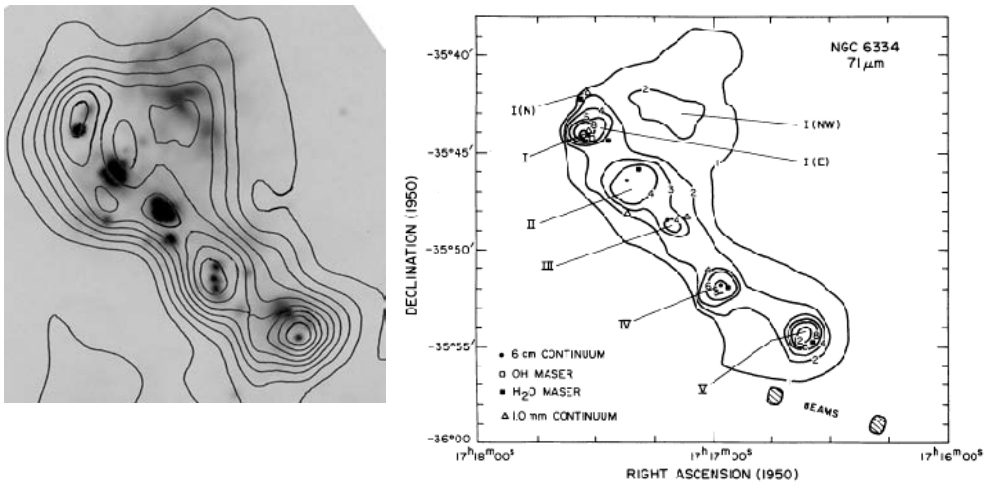

Figure 10. *Left panel*: *IRAS* HIRES 100 μm contours (adapted from Kraemer 1998) over the 21 μm *MSX* grey-scale image. *Right panel*: 71 μm map from Loughran et al (1986). The scale in both panels is the same.

The far-infrared maps obtained by Loughran et al. (1986) are comparable to the HIRES *IRAS* processed images and in all cases there is consistency with the long-wavelength *MSX* maps. This is illustrated in Fig. 10 which shows in grey scale the 21 μm *MSX* image and the HIRES 100 μm *IRAS* and Loughran et al.'s 71 μm contour plots.

A high resolution (24″) map of the 1.2 mm dust continuum emission of the whole molecular cloud and beyond, covering an area of $\sim$ 2 square degrees was performed by Muñoz et al. (2007) . The survey revealed the presence of 181 dense clumps with masses between 36 $M_\odot$ and 6×10^3 $M_\odot$ and individual sizes in the range 0.1 to 1.0 pc. Of these, 40 are located on the NGC 6334 molecular ridge and, as expected, the most massive and warmer clumps correspond to the bright far-infrared sources, as indicated in Muñoz et al.'s (2007) figure, reproduced in Fig. 11, where the 1.2 mm contours are overlaid on a 2 cm Australia Telescope Compact Array continuum map. The 250 MHz (1.2 mm) observations were carried out with the 37-channel SEST Imaging Bolometer Array (SIMBA) with a bandwidth of 90 MHz. Similar surveys were carried out by Miettinen et al. (2006) with SEST (SIMBA at 1.2 mm and SEIS at 2 and 3 mm), mapping the continuum and measuring the line emissions of ^{28}SiO, ^{29}SiO and CH_3CCH in NGC 6334 and other bright southern HII regions.

Analyses from both 1.2 mm surveys (Miettinen et al. 2006 and Muñoz et al. 2007) yield dust masses of the hot clumps (those associated with mid-infrared sources) ranging from 600 to 1500 $M_\odot$. The one corresponding to region I(N) seems to be more massive, of several hundred solar masses, implying a total dust mass for the entire ridge in excess of $1.2 \times 10^4 M_\odot$.

2.2. Large Scale Near- and Mid-infrared Maps

The first complete survey of the NGC 6334 giant molecular complex in the near-infrared was presented by Straw & Hyland (1989a). They mapped in *JHK* a large area of around 0.3 square degrees with 25″ resolution. The great majority of the 1744

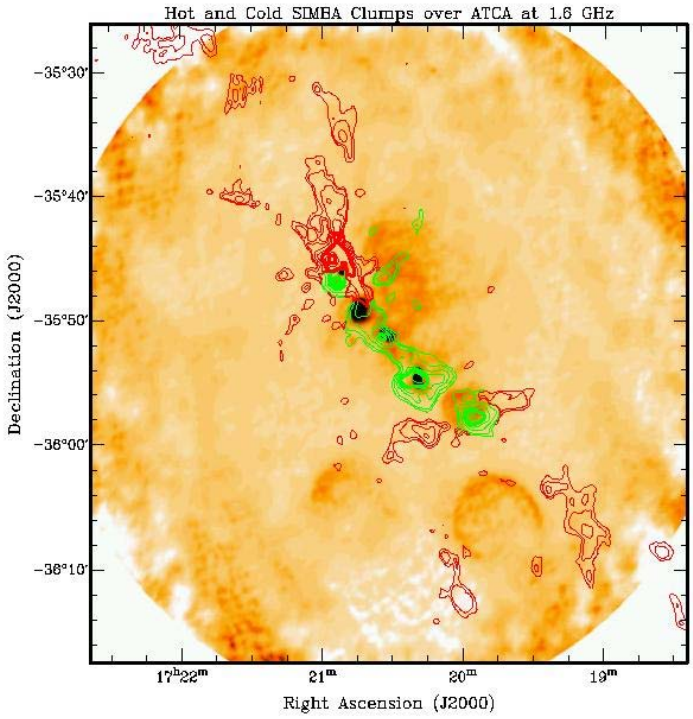

Figure 11. 1.2 mm dust emission contour map is overlaid on the ATCA radio continuum at 2 cm image. Green contours indicate warm clumps heated by embedded MSX sources while red contours are cold clumps with no associated mid-infrared source. From Muñoz et al. (2007).

sources found in K were field stars away from the areas of large extinction that characterize the dense molecular ridge. They were able, though, to provide a map of the diffuse (i.e. excluding stars) J, K emission, finding a distribution which is very similar to that of the radio continuum. This implies that this emission is dominated by hydrogen (Paschenβ, Paschenγ, Brackettγ) and possibly a few He lines. The low spatial resolution and poor sensitivity, especially with the large dust extinctions involved, prevented these authors from obtaining conclusive results about the properties of the embedded stellar population.

In an attempt to obtain evidence of a possible embedded population of young objects in the NGC 6334 complex, the same Australian group (Straw, Hyland & McGregor 1989) used the Anglo-Australian 3.9 m telescope to map in *JHK* 10 selected areas of around 5 square arcmin each that covered an important fraction of the active area along the molecular ridge and the northwestern lobe of diffuse radio and infrared emission. These single-detector observations were deeper and with much improved spatial resolution than previous large-scale attempts and were supplemented with CVF spectra of a number of red sources. Straw et al. (1989) were able to locate and study the brightest members of the young population but, again, high obscuration in the main star formation sites made the photometry at the shorter wavelengths impossible. These authors reported that the K-band luminosity functions are similar in all NGC 6334 activity centres and not very different to other large star formation complexes.

The 2MASS project provides the most complete coverage to date of the near-infrared sky and, naturally, of NGC 6334 (Figs. 4 and 7). One important conclusion from a panoramic view of the wide-field 2MASS image (Fig. 4) is the very high obscuration not just along the activity ridge, but extending to the NE of far-infrared source IV (where regions I and I(N) are located) and to the S and SW of FIR sources IV and V, just as seen in the ^{12}CO intensity map (cf. Fig. 9) of the region. In the central parts, close to the position of region III, the dense molecular ridge structure is very narrow, almost filamentary, while at both edges it widens considerably, where the molecular radial velocity becomes more negative (Kraemer & Jackson 1999). A new, deeper and with higher spatial resolution ($< 1''$) near-infrared survey of the whole molecular ridge has been obtained recently by the authors of this review with WIRC, a wide-field camera on the 2.5 m telescope at Las Campanas Observatory. Its analysis is in progress and, with it, we expect to obtain a more complete census of the embedded stellar population.

A large-scale study of all active regions of NGC 6334, based on narrow-band images, was performed by Burton et al. (2000) with SPIREX from the South Pole. They compared the distribution of the 3.3 μm emission from aromatic molecules with that of Brα (4.05 μm) from ionized gas. For region V, they also confronted these with the H_2 2.42 μm emission. Around several of the active star formation nuclei, Burton et al. (2000) found a number of bright filaments and shells of photodissociated gas emitting in the 3.3 μm line, in many cases in coincidence with strong [CII] 158 μm emission.

Large polarimetric maps in the K_s or H bands of the most extended near-infrared nebulae in NGC 6334 have been presented by Hashimoto et al. (2008). In many cases, the distribution of the polarization angles across the nebula was found to be spherical, allowing the location, and sometimes identification, of the main sources of illumination for several individual near-infrared reflection nebula. A number of other smaller and elongated nebular structures were reported to have well-aligned polarization vectors, probably suggesting the presence of one or more deeply embedded illumination sources, as in the case of the well-studied far-infrared source NGC 6334 V.

The entire NGC 6334 region was covered within the GLIMPSE survey conducted by the *Spitzer* telescope. Deep images in the four IRAC bands centred at 3.6, 4.5, 5.8 and 8 μm are now publicly available (see Fig. 5).

In addition to the global observations mentioned before, a number of detailed studies, covering practically all the infrared spectrum, have concentrated on smaller areas centred in the far-infrared and bright compact HII regions of the complex (Cheung et al. 1978, Gezari 1982, Fischer et al. 1982, Moorwood & Salinari 1981, Harvey & Gatley 1983, Harvey & Wilking 1984, Simon et al. 1985, Straw & Hyland, 1989b), Persi et al. 1996, 1998, 2000, Tapia et al. 1996, Kraemer et al. 1999, De Buizer et al. 2002). These will be described in Section 4.

3. X-ray Observations

The first X-ray detection of NGC 6334 was made with the *Einstein* satellite (Harris et al. 1990). The region was later mapped in hard X-rays with the ASCA satellite with a resolution of around $3'$ by Sekimoto et al. (2000). The five far-infrared cores, each with a typical X-ray luminosity of 10^{33} erg s^{-1}, were detected. Using *Chandra*, Ezoe et al. (2006) resolved 792 point sources, many of these concentrated on the molecular ridge. After removing the point sources, they found extended X-ray emission over a 5

$\times$ 9 pc^2 region to have a 0.5-8 Kev luminosity of 2 10^{33} erg s^{-1} (Fig. 12). The emission becomes brighter in the vicinity of the massive star forming cores, suggesting a stellar-wind shock scheme as the main mechanism to produce the extended X-ray emission. Diffuse X-ray emission were found with *Chandra* in other massive star forming regions (e.g. Townsley et al. 2003).

In an attempt to understand the origin of the X-ray emission from high-mass YSOs, Persi & Marenzi (2006) cross-correlated unresolved sources extracted from archived *Chandra*/ACIS images with infrared sources in selected areas of NGC 6334. The results differed significantly from place to place and only in NGC 6334 F were point-like X-ray sources found associated with the bright high-mass active spot. Additionally, a number of coincident X-ray and near-infrared point-like sources were reported.

So far, only two bright X-ray sources detected by *Chandra* and *Swift* have been associated with known stellar sources in this region. One corresponds to the optically visible emission line star CD -35 11482 and a second with the near-infrared source [SHM89] FIR III 13, thought to be one of the main ionizing sources of HII region C (Bassani et al. 2005).

A hard X-ray emission source in the NGC 6334 field with a non-thermal spectrum (up to 100 keV) was studied by Bykov et al. (2006) on images taken with the JEM-X and IBIS/ISGRI telescopes aboard the Gamma-Ray Astrophysics Laboratory *INTEGRAL*. In spite of the very low spatial resolution, the peak emission of the ISGRI source lies very close to the likely extragalactic radio source NGC 6334 B, to which it is probably associated. This result corroborates a similar conclusion by Bassani et al. (2005).

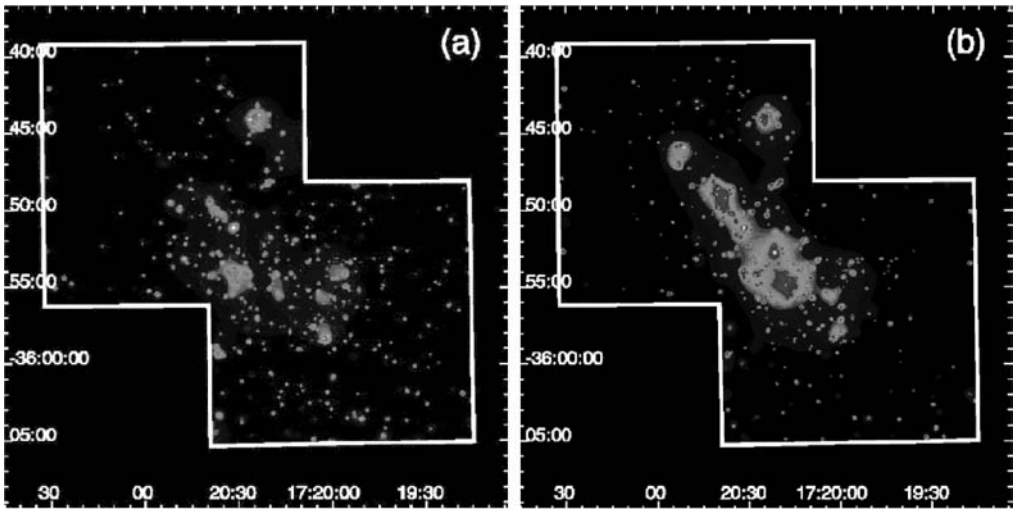

Figure 12. Smoothed X-ray images of NGC 6334 in the 0.5 - 2 keV (a) and in the 2 - 8 keV (b) bands from Ezoe et al. (2006)

4. Individual Regions

4.1. NGC 6334 North

The northern part of the cloud extends across approximately $3' \times 4'$ and contains three distinct active centres: the far-infrared source NGC 6334 I that corresponds to the ultra compact HII region labeled F by Rodríguez et al. (1982); the shell-like HII region E (Carral et al. 2002), and the 1 mm peak I(N) (Cheung et al. 1978, Gezari 1982) located $\sim 2'$ north of NGC 6334 I.

High-velocity outflows were revealed in the CO maps towards NGC 6334 I (Bachiller & Cernicharo 1990, McCutcheon et al. 2000, Leurini et al. 2006) and I(N) (McCutcheon et al. 2000). The presence of H_2O, OH and CH_3OH masers (Moran & Rodríguez 1980; Gaume & Mutel 1987; Forster & Caswell 1989; Menten & Batrla 1989; Forster 1993; Norris et al. 1993, 1998; Ellingsen, Norris & McCulloch 1996; Walsh et al. 1998; Migenes et al. 1999) in the close vicinity indicates that high mass star formation is active in the region. Two NH_3(3,3) masers, discovered by Kraemer & Jackson (1995), are located at the tips of the CO outflow in NGC 6334 I, and are coincident with knots of H_2 emission (Davis & Eislöffel 1995; Persi et al. 1996). A third NH_3 maser, also nearly coincident with an H_2 knot, is located $20''$ SE of NGC 6334 F on the

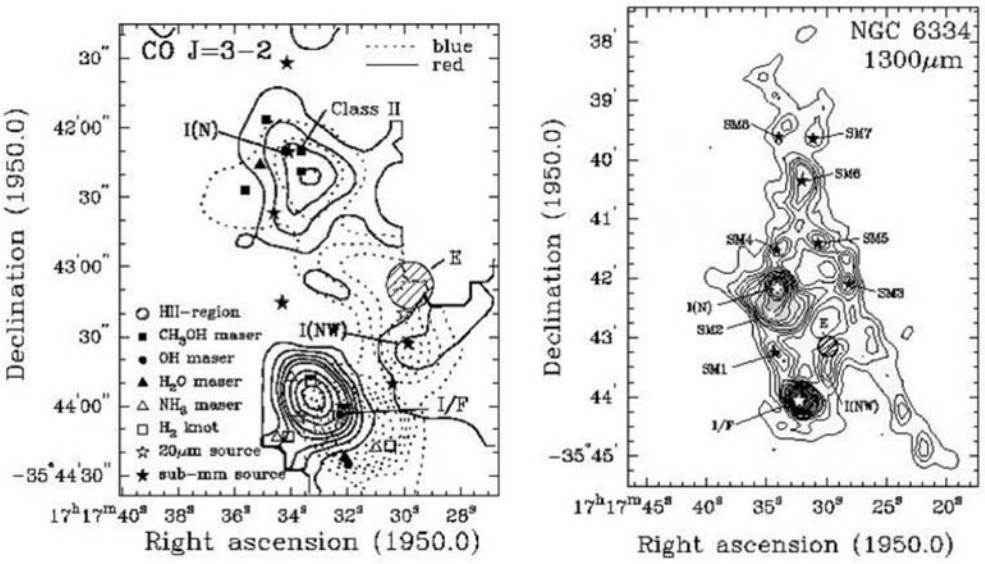

Figure 13. *Left panel*: Map of the CO J =3–2 line emission (blue and redshifted shown by dashed and continuous contours) in the northern NGC 6334 from McCutcheon et al. (2000). The principal features, NGC 6334 I, I(N), the HII regions E and F and the maser sources OH, H_2O, NH_3, and CH_3OH are indicated. Note the bipolar lobes in regions I and I(N). *Right panel*: Dust emission at 1.3 mm of NGC 6334 North from McCutcheon et al. (2000), resembling closely that of Sandell (2000) at 1.1 mm. The brightest millimeter unresolved sources correspond to the positions of UCHII regions I and I(N). The shell HII region E, without conspicuous millimeter emission, is indicated by a circle. The positions of all other continuum sources are marked with a black or white star symbols and are marked with the prefix SM.

edge of a narrow tail-shaped nebulous infrared structure seen from 1.6 to 8 μm. The shocked knot is not associated with any known molecular outflow and furtheremore, the ambient conditions that cause the observed geometry of this structure are unknown.

A "cold" submillimeter source known as NGC 6334 I(N), studied in detail by Gezari (1982), lies some $2'$ to the north of the UCHII region F (cf. Schwartz et al. 1989). It was also found to contain a weak molecular outflow (McCutcheon et al. 2000), which, additionally, is traced by high-velocity SiO line wings (Megeath & Tieftrunk 1999). Equidistant from these far-infrared sources lies the developed shell radio HII region, E (Rodríguez et al. 1982). So far there is no evidence of any physical interaction between the three active centres, which appear to be in quite different stages of early stellar evolution.

The left panel of Fig. 13 shows a CO J=3–2 map of the northern part of NGC 6334 from McCutcheon et al. (2000) with the positions of the relevant sources in this area indicated. The right panel of Fig. 13 shows the $20''$-resolution 1.1 mm map obtained by Sandell (2000). Strong thermal dust emission is evident over most of the area mapped,

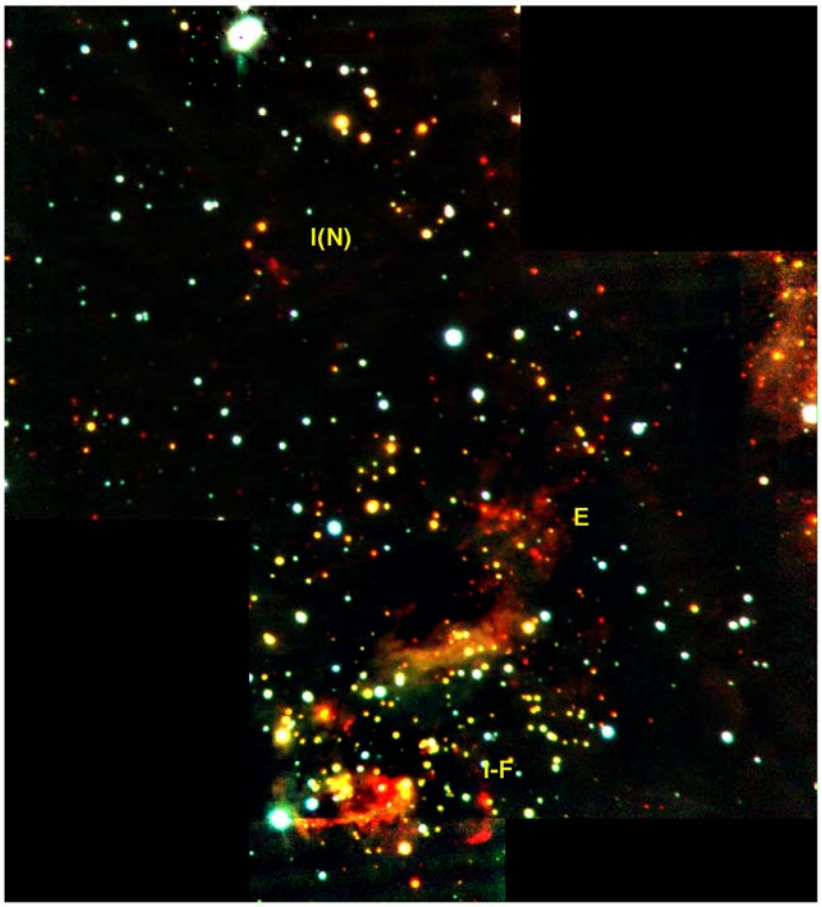

Figure 14. $196'' \times 218''$ RGB-coded image of NGC 6334 North made from J (blue), H (green), and K_s (red) mosaics. North is to the top, east to the left (from Persi et al. 2005b).

with the strongest dust emission originating from two unresolved sources. One is nearly coincident with the ultracompact HII region (UCHII) F and the far-infrared source NGC 6334 I. The second, with an extended semicircular structure to the south, is associated with NGC 6334 I(N). A ridge of diffuse dust emission is conspicuous, connecting regions I and I(N) and extending to the NW and SW. Eight additional compact millimeter and sub-millimeter sources were found embedded in the cloud. These could be massive cold starless cores that may eventually collapse to form stars (Sandell 2000).

Recently, 1.3 mm maps with a resolution of about $2''$ obtained with the Sub Millimeter Array (SMA) by Hunter et al. (2006) showed the presence of two extremely young, massive, prototrapezium-type systems, each of 4 to 7 embedded components with typical separations of around 8000 AU. These multiple dust-emission sources, described in the following sections, are located in NGC6334 I and NGC6334 I(N) and are probably in the earliest detectable phase of their (proto)stellar life.

Straw et al. (1989), in their low spatial resolution *JHK* survey, found only 30 near-infrared sources with a limiting magnitude of K=13.5. Seventeen of these were concentrated in an area of about $1'$ around the UCHII F. These authors concluded that in this region, a compact cluster of embedded sources is present. With deeper and higher-resolution near-infrared images, Tapia et al. (1996) confirmed the presence of the very young embedded cluster composed of at least 90 members (see Fig. 5 of Tapia et al. 1996), the majority of which have spectral types earlier than B4. In addition, they found a number of very red sources (some of them nebulous), associated with the region I(N) and E, previously undetected.

Recently, a mosaic of *JHK*$_s$ images covering an area of $196'' \times 218''$ of NGC 6334 North was obtained with the near-infrared camera PANIC (Persson's Auxiliary Nas-

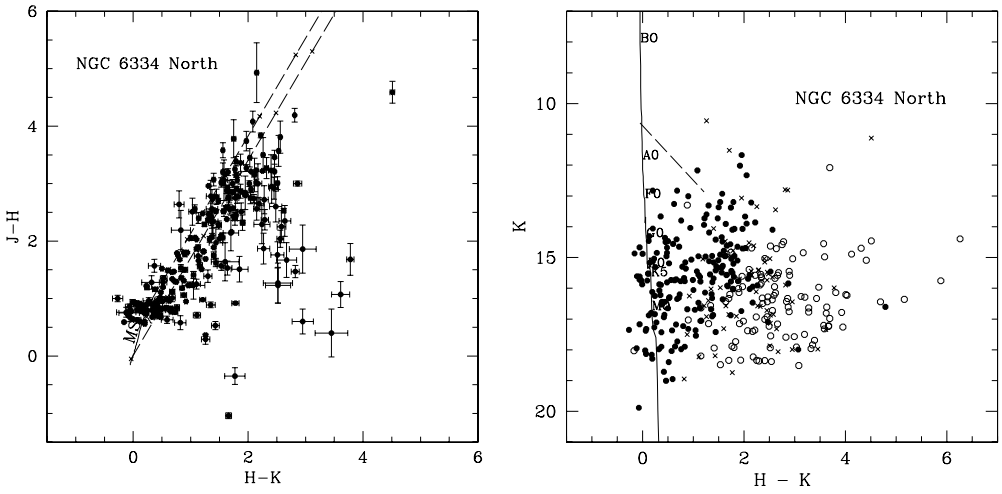

Figure 15. *Left panel*: $J - H$ versus $H - K_s$ diagram of the sources detected in the three colours towards NGC 6334 North. The solid line marks the locus of main sequence stars taken from Koornneef (1983). *Right panel*: K_s vs $H - K_s$ diagram. The reddening vector corresponding to A_V=20 is indicated with a dashed line, while the solid line is the locus of MS stars at d=1.61 kpc. Filled circles represent sources with no near-infrared excess, while crosses indicate sources with *JHK* infrared excess. Open circles are sources detected only in H and K_s.

myth Infrared Camera) on the Magellan-Clay 6.5 m telescope (Las Campanas Observatory, Chile), with a scale of 0.125″/pix and a sensitivity limit (3σ) of J=22.5, H=21.5 and K_s=19.5 (see Persi et al. 2005a, 2005b). The RGB-coded image from these mosaics is illustrated in Fig. 14. Within the quoted sensitivity limits, 405 sources were detected in K_s and 60% of them in the three colours. The $J-H$ versus $H-K_s$ and K_s vs $H-K_s$ diagrams for the measured sources are shown in Fig. 15.

From the analysis of these two diagrams, we concluded that about 30% of the sources have K_s-band excesses or $H-K_s \geq 2.5$ and, thus, are considered young stellar objects members of the complex. A simple statistical analysis of the results show that most of the young stellar cluster members have $K_s \leq$16, though a significant number of the sources with near-infrared excess have $K_s \geq 18$. Assuming a distance modulus of $m-M=11.20$ and an average value of A_K=4.0 (Tapia et al. 1996), these fainter members have $M_K \geq 2.8$. This strongly suggests the presence of a population of low-mass young stellar objects in NGC 6334 North cohabiting with high and intermediate-mass young stars in different evolutionary stages.

4.2. NGC 6334 I(N)

The region I(N) was detected at 400 μm and 1 mm by Cheung et al. (1978) and Gezari (1982). It is a dense cold core ($2.5' \times 1.5'$) with a mass of $\sim$ 2200 $M_\odot$. Sandell (2000) resolved this dense core into a bright compact (deconvolved FWHM $\sim$ 10″) millimeter source, which appears optically thick even at 1.1 mm with a surrounding, diffuse, weaker emission. The compact source emits a large fraction of its luminosity in the submillimeter ($L_{\rm bol} \sim 1.7 \times 10^4 L_\odot$, Sandell 2000), and drives a molecular outflow (see Fig. 13). The coincidence with class II CH_3OH and H_2O masers and the lack of associated compact near- or mid-infrared sources suggest that I(N) is a region where the formation of high-mass stars is at the earliest detectable phase: A protostellar object (or objects) that has just formed a hot accretion disk.

Two compact radio sources were detected towards the NGC 6334 I(N) molecular core (Carral et al. 2002). One of these lies within 0.3″ of the bright class II methanol maser G351.445+0.660 (Norris et al. 1993, Walsh et al. 1998), and of one of Sandell's (2000) bright millimeter unresolved sources. Class I methanol masers and near-infrared H_2 emission knots have been found in the vicinity of, but not coincident with, this dense nucleus (Kogan & Slysh 1998; Beuther et al. 2005; Tapia et al. 1996; Megeath & Tieftrunk 1999; Persi et al. 2005b). The extended NH_3 emission, which shows no clearly defined peak, was mapped in several transitions, first by Kuiper at al. (1995) and subsequently by Kraemer & Jackson (1999), Caproni, Abraham & Vilas-Boas (2000) and Beuther et al. (2005). The gas mass was estimated to be around 3000 $M_\odot$. The locations of several of these features are shown in Fig. 16, over a composite colour 3.6, 4.5, 5.8 μm *Spitzer*/IRAC image. Interestingly, the high-energy NH_3 (6,6) line emission was detected by Beuther et al. (2007) in the core of NGC 6334 I(N) split into two components separated by $\pm 2''$ km s^{-1} relative to the single peak observed in the NH_3 (5,5) transition. All these observational data strongly indicate that recent stellar formation has been very active within this dense core with evidence for the presence of several outflows.

With the SMA, Hunter et al. (2006) resolved Sandell's (2000) millimeter source into seven components at 1.3 mm, all but one detected later at 3.4 mm by Beuther et al. (2008) with the Australian Compact Array (ATCA). Six of the millimeter sources form a Trapezium-type configuration with typical separations of a few arc seconds (a

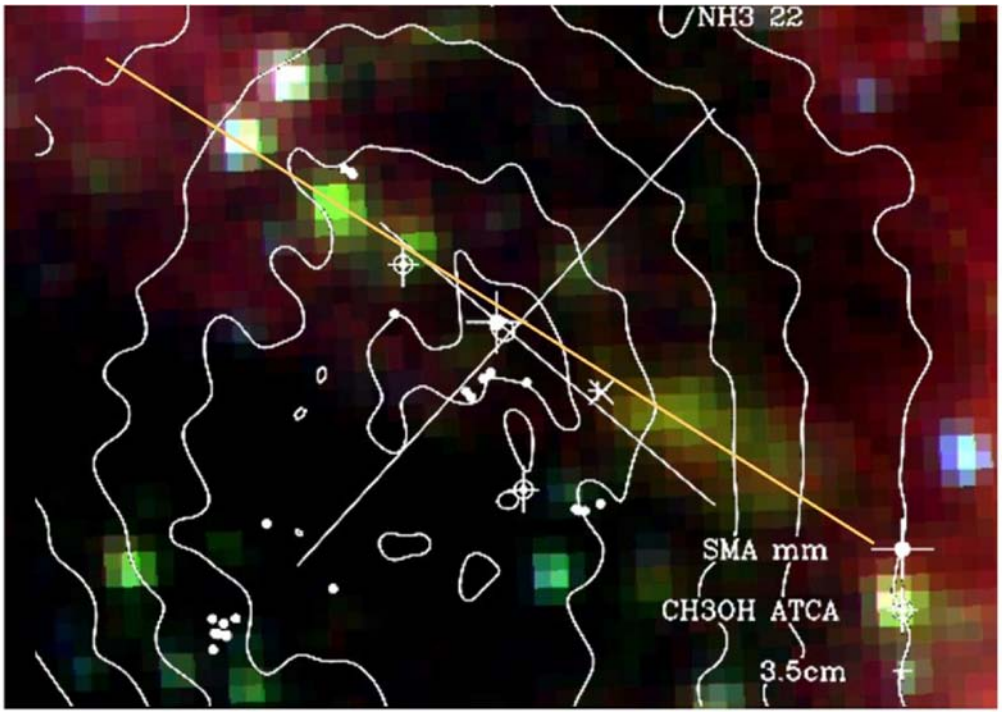

Figure 16. Contour plot, from Beuther et al. (2005), of the main hyperfine component NH_3 (2,2) line emission towards the NGC 6334 I(N) region. The methanol maser and thermal emission sites are indicated. These are superposed on a composite *Spitzer*/IRAC 3.6, 4.5, 5.8 μm colour image. The white straight lines that intersect at $\alpha = 17^{\rm h}\ 20^{\rm m}\ 55.1^{\rm s},\ \delta = -35^o\ 45'\ 05''$ outline the direction of two suspected flows as reported by Beuther et al. (2005) and Megeath & Tieftrunk (1999). The long yellow straight line, also drawn on Fig. 17, joins the 4.5 μm band emission knots and nebula, on both sides of the millimeter source. This line probably reflects more accurately the direction of the outflow. The crosses are 6.7 GHz class II CH_3OH masers and the small filled circles, 44 GHz class I CH_3OH masers. The size of the field is $68'' \times 52''$.

few thousand AU). The brightest of these objects, SMA-1 (with a derived likely mass of $10 M_\odot$, Hunter et al. 2006), looks somewhat elongated and the source was indeed resolved at 7 mm by Rodríguez et al. (2007) into three subcomponents SMA-1a, 1b and 1c separated by less than $2''$ and with likely masses of around 4, 3 and 2 $M_\odot$, respectively. These authors also found a 7 mm counterpart to the 1.3 mm source SMA-6. The observed parameters of the millimeter components are compatible with optically thin dust emission. Compact radio continuum emission was also detected at 1.3 cm by Rodríguez et al. (2007) from sources SMA-1b and SMA-4, suggesting that these are probably traces of ionized jets.

The complex structure just described is illustrated in Fig. 17 overlaid on a deep JHK image of the region. One can see geometric evidence of an outflow in the NE-SW direction, probably powered by SMA-1 and/or SMA-4. None of the millimeter components have near- or mid-infrared counterparts, at least to the limits of the available IRAC and 6.5 m telescope ground-based images. Nevertheless, 2.12 μm H_2 emission knots, and corresponding 4.5 μm IRAC counterparts, are seen aligned with the overall

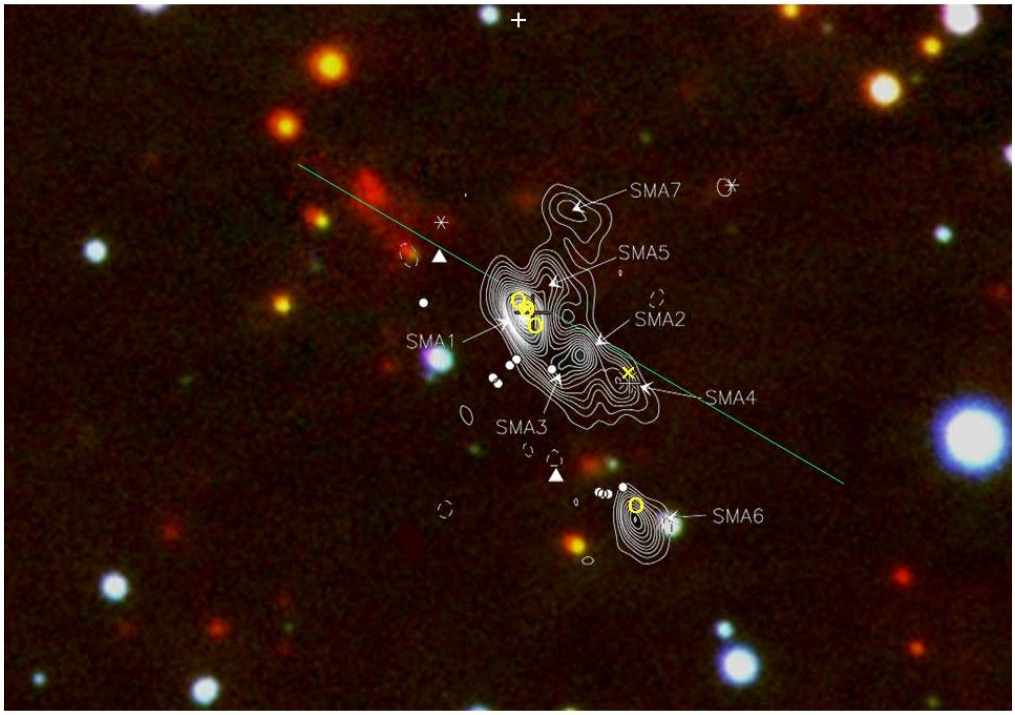

Figure 17. Magellan telescope colour-composite JHK_s image of a $74'' \times 58''$ field centred on the millimeter source NGC 6334 I(N). The non-circular red features are pure H_2 emission knots. Note that these correspond to the H_2 knots reported by Tapia et al. (1996), Megeath & Tieftrunk (1999) and Persi et al. (2005b), and are seen at 2.12 μm only on the northwestern side of the mm multiple source. The long green straight line running NE to SW is described in the caption of Fig. 16. The labeled white contours represent the 1.3 mm dust emission from a proto-trapezium-type system discovered by Hunter et al. (2006) with the SMA. Yellow open circles are compact 7 mm sources (Rodríguez et al. 2007). The filled circles and triangles mark the position of the 44 GHz and 25 GHz class I CH_3OH masers (Kogan & Slysh 1998), the small plus sign marks a 6.7 GHz class II CH_3OH maser source (Norris et al. 1993, Walsh et al. 1998). The large plus sign is a NH_3 peak (Beuther et al. 2005). The yellow crosses indicate radio HII regions (Carral et al. 2002, Rodríguez et al. 2007). The scale is the same as in Fig. 16.

elongated-shaped embedded proto-multiple stellar system towards the northeast. As pointed out by Hunter et al. (2006), another elongated "green" nebula (dominated by 4.5 μm broad-band emission, likely arising from shocked H_2) is apparent on the IRAC image (cf. Fig. 16) precisely along a putative outflow axis (long green line in Figs. 16 and 17), on the opposite side (SW) from the position of the near-infrared knots (NE side), where the extinction seems to be significantly lower, as the outflow is reaching the outer layers of the dense cloud. High-velocity red- and blue-shifted lobes in the HCN(1−0) line have been recently mapped by Beuther et al. (2008), showing a complicated (and unexplained) geometry, though some of these coincide with the H_2 nebulae.

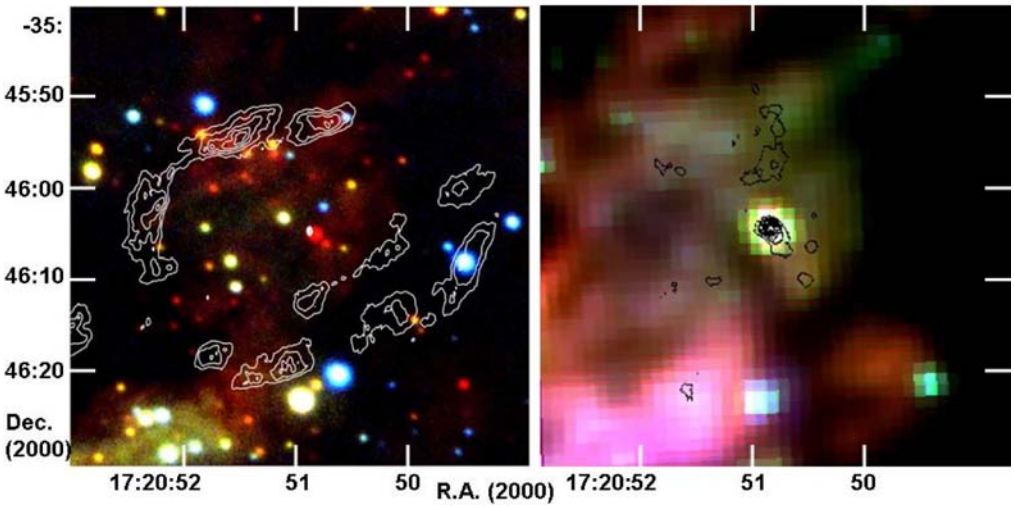

Figure 18. *Left panel*: Composite colour-coded JHK_s image of NGC 6334 E with the 3.5 cm continuum emission contours from Carral et al. (2002) overlaid. *Right panel*: Composite colour-coded *Spitzer*/IRAC (3.6, 4.5, 5.8 μm) image of NGC 6334 E with the 11.9 μm contours from Persi et al. (2005a) overlaid. Note that the scale is the same in both panels.

4.3. NGC 6334 E

This is an extended ($\sim 20''$) spherical radio HII region, first reported by Rodríguez et al. (1982), that requires an O7.5 ZAMS star to maintain its ionization. Persi & Ferrari-Toniolo (1982) searched for the near-infrared counterpart of the radio source with negative results, while Tapia et al. (1996) detected more than a dozen of very faint K-band sources and they proposed that the HII region is probably ionized by a small cluster of at least 12 B0-B0.5 ZAMS stars. The VLA map at 3.5 cm obtained by Carral et al. (2002) shows that NGC 6334 E has a shell-like morphology with a diameter of $30''$ (0.25 pc), consistent with the 18 cm map by Brooks & Whiteoak (2001) and the 1.3 cm map by Kraemer & Jackson (1999) . In addition to the shell morphology, a 3.5 cm compact unresolved ($\leq 0.5''$) source lies close to the centre of the HII region. The left panel of Fig. 18 shows the 3.5 cm radio continuum contours over a deep JHK_s image. The compact radio source is located, with an estimated error of $0.1''$, at $\alpha(2000) = 17^{\rm h}\ 20^{\rm m}\ 50.90^{\rm s}$; $\delta(2000) = -35^o\ 46'\ 04.8''$, less than $0.5''$ from the red source # 161 of Tapia et al. (1996). The new near-infrared images of this region, presented by Persi et al. (2005a) and shown in Fig. 18 (left panel), confirm the presence of an infrared nebulosity with several very red objects. In a field of $50'' \times 50''$ centred around the HII region, 8 sources show near-infrared excess, and about 20 have $H - K_s \geq 2.5$. A number of nebulous emission knots within the radio shell, seen predominantly at 2.2 μm (K-band) and at 4.5 μm (IRAC channel 2-band), may be signatures of embedded shocks and outflows (Fig. 18).

The very red source ($H - K_s = 6.3$) coincident with the central compact radio source is Tapia et al.'s (1996) source #161. It was detected also at 11.9 μm with the mid-infrared camera TIMMI2 on the 3.6m ESO telescope and in the L-band by Burton et al. (2000). Naturally, the source is very bright in all IRAC bands, being the brightest point

source of the region at 8 μm (right panel of Fig. 18). The near- to mid-infrared spectral energy distribution of this object (Persi et al. 2005a) rises very steeply with a spectral index $\alpha_{\rm IR} = 2.1$ and an infrared luminosity $L_{\rm IR} = 8.4\ L_{\odot}$. These values suggest the presence of a Class I low mass young stellar object at the centre of NGC 6334 E. This object cannot be the sole source of ionization of the entire shell-shaped HII region, consistent with the lack of strong millimeter and submillimeter emission in Sandell's (2000) maps. As suggested by Tapia et al. (1996), there must be additional stellar sources in the zone.

The morphology of the HII region NGC 6334 E suggests a state of evolution considerably later than its neighbours, regions I and I(N). For this reason, it will be enlightening to study further the nature of the embedded, very young red objects which seem to be associated with NGC 6334 E.

4.4. NGC 6334 I = F

The far-infrared source I is associated with the ultracompact HII region F (Rodríguez et al. 1982). It has a cometary shape in the radio (De Pree et al. 1995; Ellingsen et al. 1996), millimeter (Carral et al. 1997; Carral et al. 2002), near-infrared (see Fig. 19) and mid-infrared (Persi et al. 1998; Kraemer et al. 1999; De Buizer, Piña, & Telesco 2000; De Buizer et al. 2002), with its head pointing to the northwest and the tail running to the southeast. After the discovery by Moran & Rodríguez (1980) of an H_2O maser source in this region, high-resolution surveys (Forster 1992; Migenes et al. 1999) revealed several clusters of this kind of masers in cohabitation, though not coinciding, with OH (Gaume & Mutel 1987) and CH_3OH (Ellingsen et al. 1996; Walsh et al. 1998). All are distributed (see e.g. Fig. 5 of De Buizer et al. 2002) along the well-defined northern

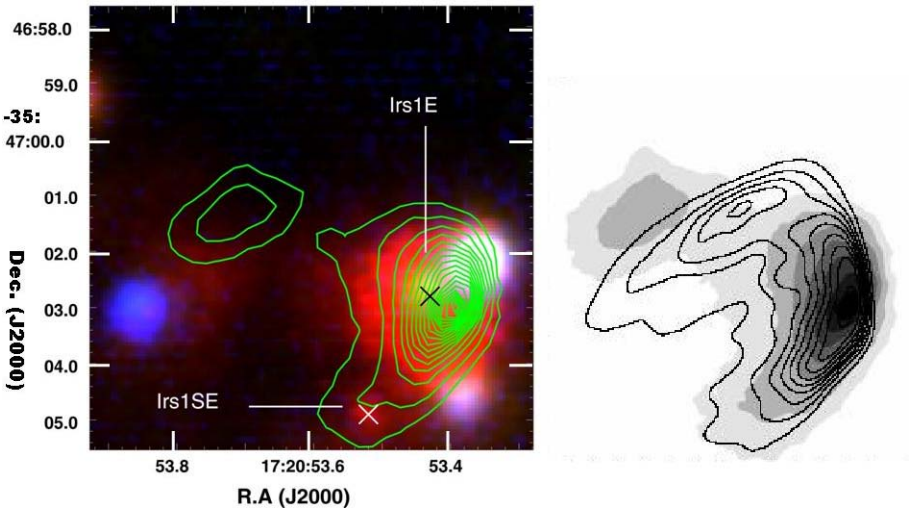

Figure 19. *Left panel*: The 18 μm contour map (green lines) from De Buizer et al. (2002) superimposed on the colour composite JHK_s-band image of NGC 6334 F. The crosses mark the position of the two *Chandra* X-ray sources in the field as reported by Persi & Marenzi (2006). *Left panel*: The 3.5 cm radio-continuum map of Carral et al. (2002) (contours) with the 18 μm grey-scale image. The scale in both panels is the same

and eastern edges which delimit the interaction zone of the expanding HII region with the dense molecular core (Kraemer et al. 1999).

Three extended mid-infrared sources were reported in the 20 and 30 μm maps of this region by Harvey & Gatley (1983). The brightest of these (IRS-I-1) coincides with the radio peak, while the other two sources, designated IRS-I-2 and IRS-I-3, lie 6″ to the northwest and 18″ to the east of IRS-I-1, respectively.

IRS-I-1 was found to have two mid-infrared components (designated I:KDJ1 and 4 by Kraemer et al. 1999, and IRS-I-1 and G351.42+0.64:DPT00 2 by De Buizer et al. 2002). Four near-infrared sources were found within 3″ of the IRS-I-1 peak by Persi et al. (1996). De Buizer et al. (2002) presented a detailed comparison between the radio, near-infrared and their mid-infrared images with similar spatial resolution. A good morphological coincidence is evident (see Fig. 19), and in particular, the near-infrared source IRS1E, coinciding with the mid-infrared peak, is considered to be the object most probably responsible for the heating and ionizing of the UCHII region. A second source, IRS1SE, so red that it was detected only in K_s, lies in an area of diffuse mid-infrared emission. Fig. 19 shows comparisons between the high resolution JHK_s-band, the radio-continuum and the 18 μm images. IRS1E and SE have been identified by Persi & Marenzi (2006) *Chandra* X-ray emitters, and are marked in Fig. 19 (left panel). IRS1E shows a very steep spectral energy distribution with a spectral index $\alpha_{\rm IR} = 3.8$ and an infrared luminosity $L_{\rm IR} = 3 \times 10^3\ L_\odot$. The adjacent mid-infrared source G351.42+0.64:DPT00 2 (KDJ 4) towards the east appears to be a clump of dust. Its morphology, temperature and opacity maps obtained by Kraemer et al. (1999) suggest that I:KDJ 4 is not self-luminous, but rather heated externally by the HII region.

The "bluer" near-infrared sources IRS1W and IRS1SW (Persi et al. 1996) seem spatially related to a couple of groups of methanol masers on the sharp western edge of the UCHII region. These near-infrared sources cannot be reddened stars seen directly, and their nature remains unclear. The mid-infrared source IRS-I-3 (=KJD3) towards the east has been resolved and seen to have an hourglass-like shape with two distinct peaks (Persi et al. 1998; Kraemer et al. 1999; De Buizer et al. 2002). The hourglass-like shape may be caused by a torus or disk of dust surrounding a young embedded protostellar object.

The observed characteristics of the UCHII region NGC 6334 F with its associated maser, infrared and X-ray sources, are naturally explained by a centrally-heated shell of ionized gas that is expanding relatively freely towards the east and along the line of sight. In contrast, towards the northwest it has encountered, and is strongly interacting with, a very dense molecular clump, a geometry that explains the sharp edge of the HII region and the presence of several aligned signposts of shocks and gas compression along this border. The dense core was mapped by Kraemer & Jackson (1995) and Jackson et al. (1999) in NH_3 (3,3), and later in several other transitions of NH_3 and also in CH_3OH and CH_3CN by Beuther et al. (2005, 2007, 2008) These reveal a double-peaked emission structure located a few arcseconds (a few AU) from the edge.

This double, dense core is at the centre of well-collimeted red and blue lobes of CO that characterize a high velocity bipolar outflow (Bachiller & Cernicharo 1990; McCutcheon et al. 2000; Leurini et al. 2006), also evident in the HCN(1−0) 3.4 mm line.(Beuther et al. 2008). The tips of the outflow are marked by shock-excited H_2 emission knots and coinciding NH_3 (3,3) masers (Kraemer & Jackson 1995; Tapia et al. 1996; Beuther et al. 2007), as illustrated in Fig. 20.

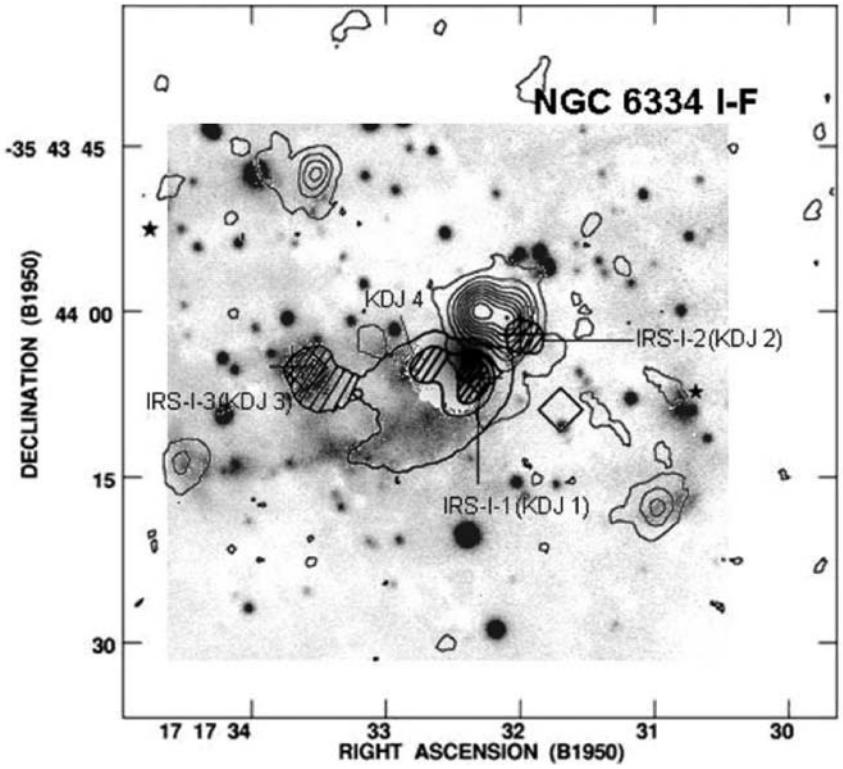

Figure 20. K_s-band image of the NGC 6334 I region (grey scale) with NH_3(3, 3) emission (contours) and the 20.6 μm emission (labeled hatched areas with heavy contours) from Kraemer et al. (1999). The three compact sources are NH_3(3, 3) masers, coinciding with H_2 2.12 μm knots (Kraemer & Jackson 1995, Persi et al. 1996).

The discovery of an extremely young multiple system of four components in a Trapezium-type configuration by Hunter et al. (2006) provides another (see also the case of NGC6334 I(N)) very important evidence that massive stars *are formed* in structures with this kind of configuration (cf. Poveda 1977). Using the 6-antenna SubMillimeter Array on Mauna Kea, these authors obtained a sub-arcsec resolution map at 1.3 mm of NGC 6334 I that is shown in Fig. 21 together with other features observed at several wavelengths.

Sandell's (2000) single-dish "point-like" ($< 18''$) 0.8 and 1.1 mm source which implied the presence of a heated dust cloud ($T_{\rm d} > 100$ K) of mass of $\sim 200 M_\odot$, was resolved by Hunter et al. (2006) into four compact sources (plus diffuse emission) with separations of a few arcsec, corresponding to a few thousand AU, and likely individual masses between 10 and 40 $M_\odot$. Interestingly, the two brightest components correspond to the two primary NH_3 peaks that mark the densest clumps with associated H_2O masers (SMA 1) and class II CH_3OH. The extended mid-infrared source IRS-I-2 (= KDJ2) lies close to the millimeter component SMA 2, but its morphology and offset position rules out that this warm dust knot is internally heated (De Buizer et al. 2002, Hunter et al. 2006). The almost exact, symmetrical alignment of the CO high-velocity lobes,

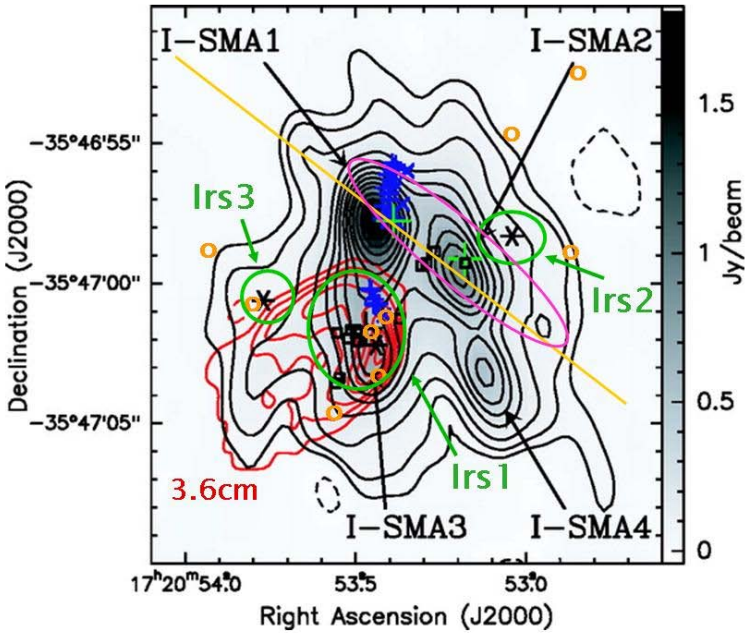

Figure 21. 1.3 mm dust emission (black contours and grey scale) as reported by Hunter et al. (2006), towards NGC 6334 I. Red contours mark the 3.6 cm continuum emission, blue crosses and plus signs are H_2O masers (Migenes et al. 1999, Forster 1993), black open squares are class II CH_3OH masers (Walsh et al. 1998), green plus signs are NH_3 thermal emission peaks and the cyan ellipse represents the elongated hot maser $NH_3(6, 6)$ emission (Beuther et al. 2005, 2007), the asterisks are centres of extended 20 μm emission sketched by green ellipses (De Buizer et al. 2000, 2002) and the pink circles mark very red point-like near-infrared sources (Persi et al. 1996). The yellow straight line joins the 2.12 μm and NH_3 maser and 2.12 μm H_2 emission knots (see Fig. 20).

the NH_3 (3,3) and (6,6) masers and H_2 near-infrared emission knots (Figs. 20 and 21) strongly suggest that SMA 2 is the main engine of the bipolar outflow.

The faintest 1.3 mm source (SMA 4), on the other hand, has no infrared or radio counterpart. The observed millimeter flux from these objects is pure thermal dust emission, according to Hunter et al. (2006). In contrast, these authors estimate that the millimeter radiation from the fourth millimeter component, SMA 3, mapped at 7, 3, and 1 mm (Carral et al. 1997, Hunter et al. 2006, Beuther et al. 2008, respectively) is clearly associated with the UCHII region E and these observations reflect a combination of Brehmstrahlung and thermal dust emission. The millimeter spectra of NGC 6334 I obtained with large beams that cover the whole nucleus (McCutcheon et al. 2000; Thorwirth et al. 2003; Schilke et al. 2006) indicates an environment that is rich in molecular line emission, including methanol, methyl formaldehyde and dimethyl ether.

Important questions remain open in the above picture, in particular concerning the variety of conditions that prevail in each of the four millimeter components of this extremely young multiple system. It would be difficult to imagine a non-coeval formation of all members of a close multiple stellar system. For example, what causes that SMA 4 is not seen embedded in a density peak in sharp contrast with SMA 1 and SMA 2? Still

more puzzling, why is SMA 3, the UCHII region NGC 6334 F, so different than the other three, in particular with SMA 4, which has a similar dust mass? Is this caused by significant variations of the accretion rates from one condensation to the other that in turn greatly modify the evolutionary timescales?

4.5. NGC 6334 II = D

Coinciding with the far-infrared peak II of Breen et al. (1979), Rodríguez et al. (1982) found an extended ($\approx 40''$) spherical HII region (D). Their radio fluxes implied at least one ionizing (ZAMS) star of spectral type O6.5 to power the HII region. This source was first observed in the radio continuum by Schraml & Mezger (1969) and later by Brooks & Whiteoak (2001).

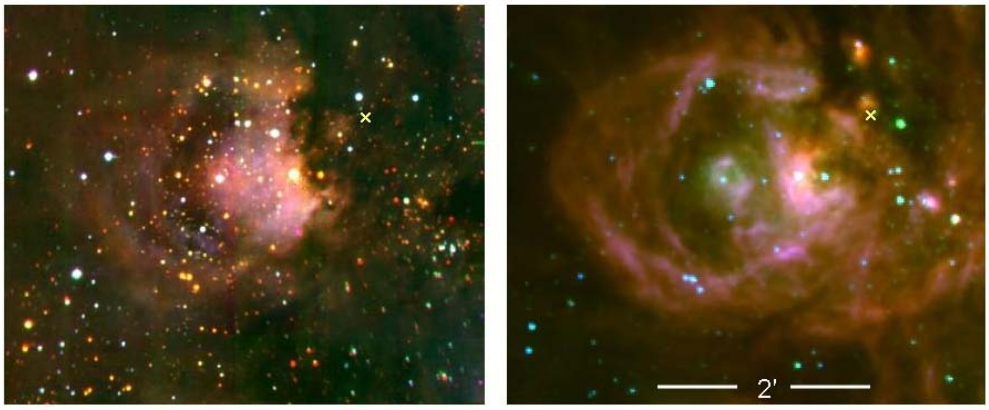

Figure 22. Composite DuPont/WIRC JHK_s (left panel) and *Spitzer*/IRAC 3.6, 4.5, 8 μm (right panel) colour images of NGC 6334 II. The scale is the same for both panels. The cross indicates the position of the water vapour maser detected by Moran & Rodríguez (1980).

Extended emission at 3.6 μm associated with the HII region was also detected by Persi & Ferrari-Toniolo (1982), and a similar nebulosity was observed at 2.2 μm by Straw et al. (1989). The detailed morphology in the near- and mid-infrared is seen on recent Las Campanas/WIRC JHK_s and *Spitzer*/IRAC 3.6, 4.5, 8 μm images, as displayed in Fig. 22. It is clear that the shell structure of the developed HII region is very similar in the near- and mid-infrared, and also in the radio continuum (cf. Brooks & Whiteoak 2001). The bright near-infrared point source, right at the centre of the ionized shell, first reported by Straw et al. (1989; Irs 24), seems to be the main star responsible for ionizing the gas and causing its expansion. These authors assigned an O-spectral type to this star and it is natural to assume that its strong radiation and stellar wind clearly have swept up the material in the central region. Indeed, the central cavity not only looks quite empty of dark material in the near-infrared, but also exhibits a marked density minimum, or "hole", in the distribution of CO and other molecules, evident on the maps by Kraemer & Jackson (1999) and Zhang et al. (2007). This also explains the fact that the extinction towards the HII region D is considerably low, as some of the gas is seen even on the red images (north of the visible stars N31 and N32) presented in Figs. 1 and 2.

It appears that the expansion of the shell, with all the swept-up material, is triggering the formation of a new generation of stars at the western edge, where it strongly interacts with the denser molecular cloud. Indeed, this is the position of the far-infrared peak II, coincident with a red near- and mid-infrared point source surrounded by a nebulosity of similar colours. A water vapour maser, discovered by Moran & Rodríguez (1980) is located some $30''$ to the north of this spot. Note in the left panel of Fig. 22 (JHK_s image) the presence of what appears to be a very highly reddened star cluster some $1''$ to the west of the far-infrared peak, near the limit of the field. The analysis of this infrared data by the authors is in progress. By comparing Brγ and H_2 Magellan-telescope images of the central field, we find no clear evidence of shocks and outflows. The results described here suggest that NGC 6334 D is one of the oldest regions on the molecular ridge, though the expansion of the HII region seems to be triggering a new generation of stars, as in, e.g., S 104 (Deharveng et al. 2003).

4.6. NGC 6334 III = C

The non-spherical and extended radio-continuum source C, of size $\sim 40''$, was first mapped by Rodríguez at al. (1982), and later by De Pree et al. (1995) and Brooks & Whiteoak (2001). Its position coincides with the far-infrared peak III, near the (projected) centre of the dense molecular ridge. This source has no known maser emission of any species nor any outflow activity. The near-infrared emission, first observed by Persi & Ferrari-Toniolo (1982) and Straw et al. (1989), and the mid-infrared emission (*Spitzer*) has roughly the same shape and size as the radio emission. In addition, Straw et al. (1989) identified a bright near-infrared source (Irs 13), located in the northern part of NGC 6334 C, as the excitation source for the radio and IR continuum emission as well as for the optical nebulosity in the region. Nevertheless, new DuPont/WIRC *JHK* and IRAC images indicate that the true main exciting source probably lies at the centre of the HII region (Fig. 23). This central source shows considerable near-infrared excess. In addition, several very red sources are located to the west of the HII region and could indicate the presence of a young stellar cluster. The analysis of the new infrared images is in progress.

4.7. NGC 6334 IV = A

In the radio continuum, NGC 6334 IV (radio source A) has a small ($\sim 20''$) shell-like structure, first described by Rodríguez et al. (1982), that seems to be rotating (De Pree et al. 1995). Two large radio bipolar plumes that extend some $2'$ (Rodríguez et al. 1988) are seen to the north and south of NGC 6334 A. The same bipolar structure is observed from the near- (Fig. 24) to the far-infrared frequencies (Kraemer et al. 1999, and *IRAS, MSX* and *Spitzer* maps). The obscured central region is characterized by the presence of a massive and clumpy molecular disk mapped in NH_3 by Kraemer et al. (1997), two bright young stellar objects (IRS 19 and IRS 20; Harvey et al. 1987), OH and H_2O masers (Rodríguez et al. 1988), several ammonia clumps, and a bright millimeter and sub-millimeter emission (Sandell 1999). High resolution mid-infrared images by Kraemer et al. (1999) showed that IRS 19 and IRS 20 are extended and multiple. These sources are also resolved in the near-infrared (Persi et al. 2000). In particular, IRS 20 has been found to be a system composed of at least two ZAMS B2-B3 stars. This object is close to the H_2O maser and the CS emission peak, implying the presence of a dense nucleus. The far-infrared luminosity is found to be $\sim 10^5 L_\odot$ (Kraemer et al. 1997).

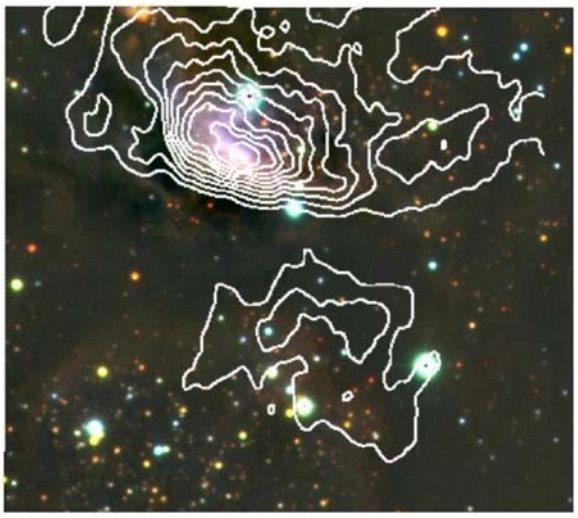

Figure 23. "True colour" image of NGC 6334 III(C) made from J (blue), H (green) and K_s (red) DuPont/WIRC images. The field size is $4' \times 3'$ and is centred at (J2000) $\alpha = 17^{\rm h}\ 20^{\rm m}\ 30.8^{\rm s}$, $\delta = -35^o\ 52'\ 02''$. The contours represent the continuum 18 cm emission, from Brooks & Whiteoak (2001).

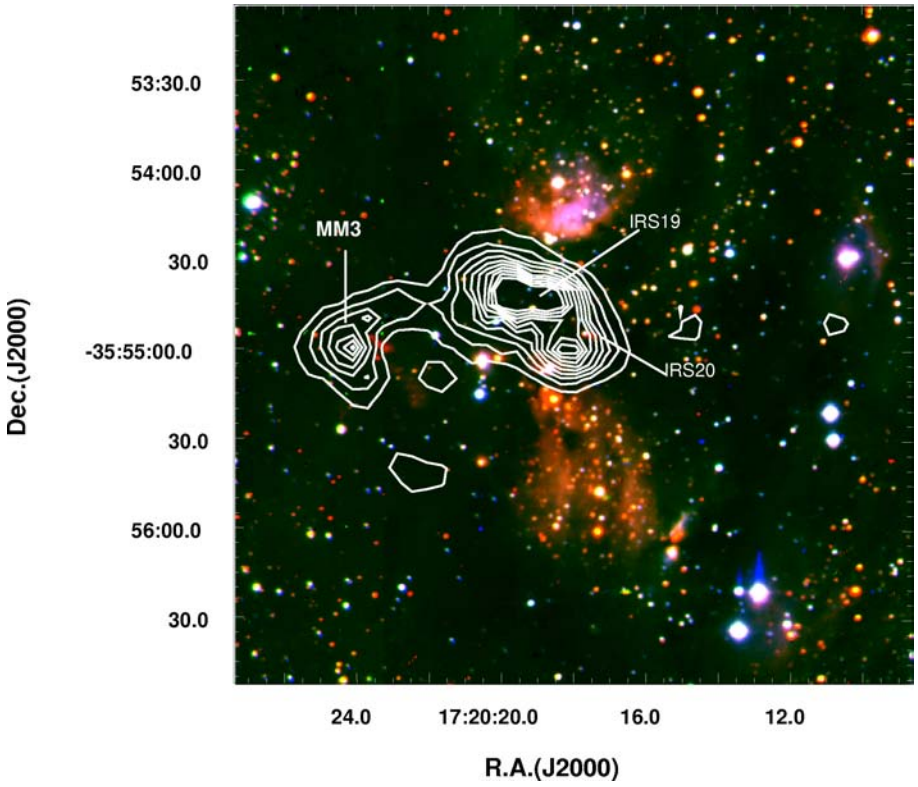

Figure 24. "True colour" image of NGC 6334 IV made from J (blue), H (green) and K_s (red) individual images from Persi et al. (2000). The contours show the 1.1 mm emission of Sandell (1999).

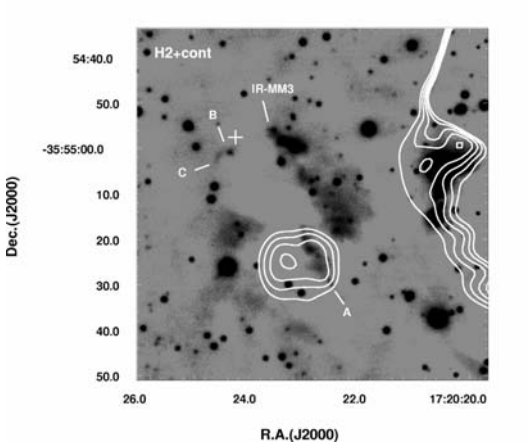

Figure 25. H_2 + continuum image of NGC 6334 IV (MM3) region. The contours represent the 3.6 cm radio continuum. The H_2 knots A,B, and C are indicated. The symbol (+) marks the position of the sub-mm peak (Persi et al. 2008).

Persi et al. (2000) claimed that there is no evidence of a *developed* stellar cluster, but only of the presence of a small number of luminous (O-B2) young stellar objects. In accordance with Kraemer et al. (1997), they proposed that these YSOs are embedded in the densest part of the molecular cloud that is at the centre of a giant bipolar structure seen in the radio and the infrared. This morphology is the result of the effect of massive stellar winds originating from a source at the centre of a dense molecular toroid which, in turn, collimates the outflow material giving rise to two lobes of thermal gas and dust emission. Several sections of the infrared nebula was found by Hashimoto et al. (2008) to be highly polarized, most conspicuously, the SW bipolar reflection nebula (labeled IRN IV-5), described in detail by Persi et al. (2000).

A new centre of active star formation was found to the east of the central region (Persi et al. 2000), as indicated by the presence of strong sub-millimeter emission, in particular with the emission peak named MM3 (Sandell 1999, Fig. 24). The results of the analysis of new sub-arcsec infrared observations that include narrow-band H_2 and Brγ and mid-infrared images (Persi et al. 2008) indicate the presence of a number of H_2 emission knots (the brightest three, A, B and C indicated in Fig. 25) suggesting the presence of collimated outflows. Knot A is very close to the radio continuum source G351.25+0.65, while knots B and C are in the vicinity of the sub-millimeter peak and may be excited by the nearby bright mid-infrared source IR-MM3 at the apex of an extended infrared nebulosity. This Class I object has a bolometric luminosity of around $10^3 L_\odot$ (Persi et al. 2008) and has an associated OH maser source located some $3''$ east of IR-MM3 (Brooks & Whiteoak 2001).

4.8. NGC 6334 V

NGC 6334 V is the southernmost far-infrared continuum source detected by McBreen et al. (1979). It appears unresolved at a resolution of $3'$, and the peak is located $\sim 30''$ from IRAS 17165–3554. This region has faint radio emission that arises from three or four compact sources (Rengarajan & Ho 1996; Jackson & Kraemer 1999). Methanol and hydroxyl masers have been detected in a small area, close to the far-

infrared peak (Walsh et al. 1998; Braz & Epchtein 1983; Argon et al. 2000; Brooks & Whiteoak 2001). NGC 6334 V coincides precisely with the position of a peak of CO (2-1) emission (Jackson & Kraemer 1999).

NGC 6334 V has been extensively studied at near- and mid-infrared wavelengths (Persi & Ferrari-Toniolo 1982; Fischer et al. 1982, Harvey & Gatley 1983; Harvey & Wilking 1984; Simon et al. 1985; Wolstencroft et al. 1987, Straw et al. 1989; Kraemer et al. 1999; Burton et al. 2000; Alvarez et al. 2004, Hashimoto et al. 2007, 2008). These observations indicate that source V contains several compact dust condensations as well as a near-infrared bipolar nebula within a small region, of size $\sim 30'' \times 8''$. The elongated morphology of this emission, from 1.6 to 18.8 μm, is displayed in Fig. 26. Four compact mid-infrared sources (V:KDJ 1-4) were detected at both 12.5 and 20.6 μm by Kraemer et al. (1999; their Fig. 6). Three of these correspond to the near-infrared sources IRS V-1, IRS V-2, and IRS V-3 of Simon et al. (1985), detected at 3.5 μm. The mid-infrared sources V:KDJ 1 and 4 seem to be associated with the faint radio sources R E-2 and R E-3 of Rengarajan & Ho (1996). Consistent with this, mid-infrared narrow-band images with higher spatial resolution taken with the VLT and VISIR reveal a complex structure with several compact sources surrounded by diffuse emission (Fig. 26). KDJ 1 (= IRS V-1) shows a very steep spectral energy distribution with deep absorption bands at 3.1 and 9.8 μm (Fischer et al. 1982). Source KDJ 3 was resolved into two red components with a separation of $1''$ at 3.6 and 5.0 μm by Hashimoto et al. (2007), and source KDJ 4 coincides with two NH_3 (3,3) clumps (Kraemer et al. 1999). The latter is associated with an OH maser, and lies very close to a CH_3OH maser position (Walsh et al. 1998). All these features are summarized graphically in Fig. 26. Infrared polarimetric studies have shown that the nebular lobes are highly polarized, implying a reflection origin (Fischer et al. 1982, Nakagawa et al. 1990, Chrysostomou et al. 1994, Hashimoto et al. 2007, 2008). On the other hand, the low-resolution large-aperture K-band spectrum of the source shows prominent H_2 emission lines at 2.12 and 2.4 μm (Simon et al. 1985). This is confirmed by the enhanced brightness of the elongated structure of NGC 6334 V in the 4.5 μm IRAC band (channel 2) (Fig. 27). Interestingly, an unresolved (both spatially and spectroscopically) knot of (probably maser) NH_3 (3,3) emission was reported by Kraemer & Jackson (1995) some $30''$ NW of region V.

4.9. Other Centres of Star Formation Activity

G351.20+0.70 This radio HII region was first detected at 6 cm by Moran et al. (1990) with the VLA while they were probing the nature of the stronger compact radio source NGC 6334 B (which proved to be an extragalactic object, thus unrelated to NGC 6334).

Observations of G351.20+0.70 at 3.5 cm by Jackson & Kraemer (1999) show that G351.20+0.70 is part of a much larger ring or shell of radio emission with a radius of approximately $1'$ (0.4 pc). Additional 6 and 18 cm maps were provided by Sarma et al. (2000) and Brooks & Whiteoak (2001). The western portion of G351.20+0.70 looks arclike, and overlaps with the position of NGC 6334 V (see Fig. 27). The nearly spherical shell of radio emission, very similar to that seen in Brα (Burton et al. 2000), suggests that the H II region is being ionized by one or more sources near the shell's centre. Recent JHK and *Spitzer*/IRAC photometry shows four sources with considerable infrared excess in the central zone of the shell, two of which show extended morphologies in the 3.6, 4.5, 5.8 and 8 μm IRAC images. Straw et al.'s (1989) Irs 41 is the one closest to the geometrical centre of the HII region and probably is the primary

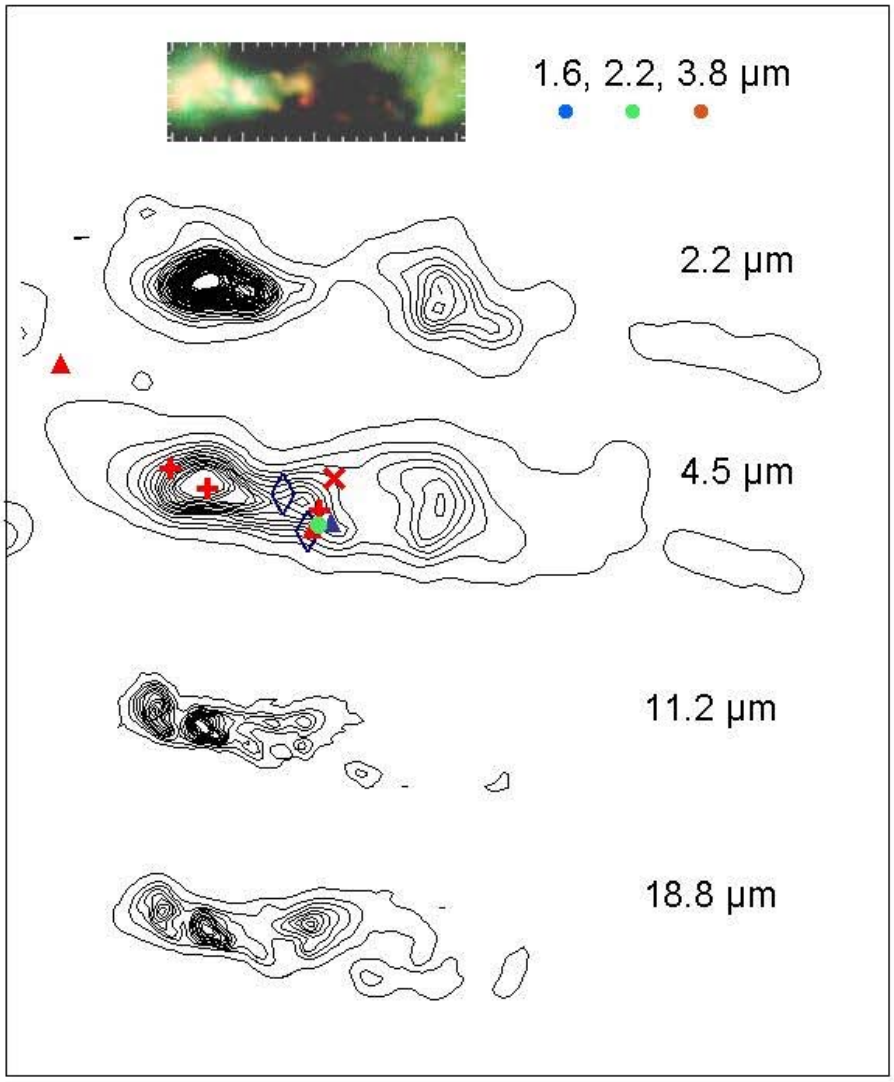

Figure 26. Contour plots of the bipolar infrared source NGC 6334 V at 18.8 and 11.2 μm (VLT/VISIR), 4.5 μm (*Spitzer*/IRAC), 2.2 μm, and a high resolution ($0.3''$) colour-composite 1.6, 2.2 and 3.8 μm map (from Hashimoto et al. 2007). The positions of several radio sources are marked on the 4.5 μm contour map: 2 and 6 cm (red plus signs; Rengarajan & Ho 1996; Jackson & Kraemer 1999), *MSX* source position (red cross), OH maser (blue triangle; Brooks & Whiteoak 2001), CH_3OH maser (red triangle; Walsh et al. 1998), H_2O maser (green dot; Forster & Caswell 1989) and $NH_3(3,3)$ (blue diamonds; Kraemer & Jackson 1995). All displays are aligned and have the same scale. The horizontal size of the box is $78''$.

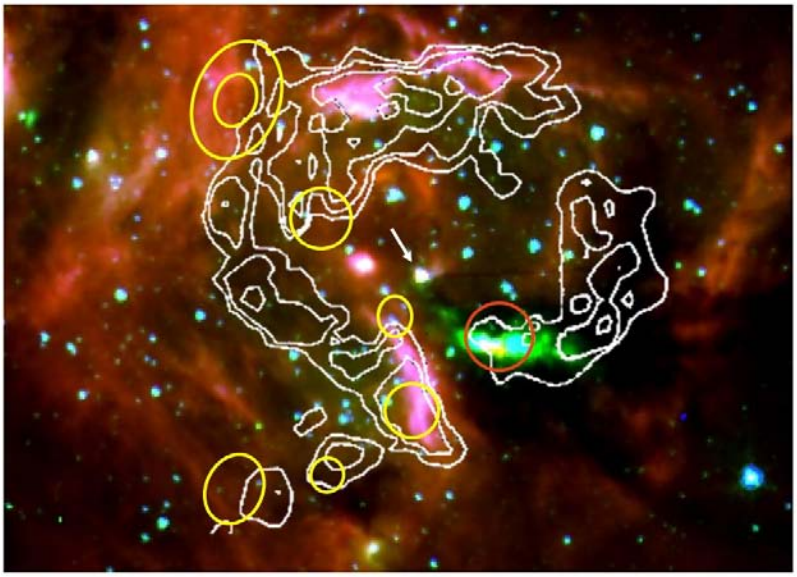

Figure 27. Composite colour image with *Spitzer*/IRAC images at 3.6, 4.5 and 8 μm of a $6.0' \times 4.5'$ region which includes G351.20+0.70 and NGC 6334 V. Overlapping white contours show the 3.5 cm continuum emission of the shell HII region G351.20+0.70, the red circle marks the maximum of CO ($2 \rightarrow 1$) emission and the yellow ellipses represent the peaks of [CII] 158 μm emission that indicate PDRs (from Jackson & Kraemer 1999). The arrow points to the infrared-excess star IRS 41 (Straw, Hyland & McGregor 1989) which may be the main contributor to the ionization of G351.20+0.70. The centre is at (J2000) $\alpha = 17^{\rm h}\ 20^{\rm m}\ 01.0^{\rm s}$, $\delta = -35^o\ 57'\ 21''$.

energy source for its ionization and expansion (e.g., Jackson & Kraemer 1999). Fig. 27 shows a composite colour image composed with the *Spitzer*/IRAC images at 3.6, 4.5 and 8 μm of a $4.5' \times 6.0'$ region that includes G351.20+0.70 and NGC 6334 V overlaid with the radiocontinuum (3.5 cm), CO(2-1) and [CII] (150 μm) emission.

It is important to note the fragmentary structure of the ionized shell and that NGC 6334 V, embedded in a dense molecular clump (Kraemer & Jackson 1995, Jackson & Kraemer 1999), is at the edge of one of these fragments (Fig. 27) in a region of extremely high obscuration. It is easy to contemplate, again, that the result of the interaction of the expanding HII region with a very dense molecular clump, led to the formation of a compact stellar cluster, NGC 6334 V. The presence of a photodissociation front, marked by the enhanced PAH emission (the bright elongated structure in the 8 μm IRAC image) and coincident with [CII] 158 μm peaks (Jackson & Kraemer 1999) is compatible with this scenario.

G351.39+0.73 and G351.44+0.73 These are two compact radio sources reported in the 21 cm NVS Survey (Condon et al. 1998) located to the north of far-infrared sources II and III, respectively. These stand out over an extended and diffuse emission in Sarma's (2000) and Brooks & Whiteoak's (2001) maps that look quite similar to the extended mid-infrared emission mapped by *MSX*. Only a faint, diffuse 3.6 to 8 μm emission is apparent on IRAC images towards both sources. We believe that these two

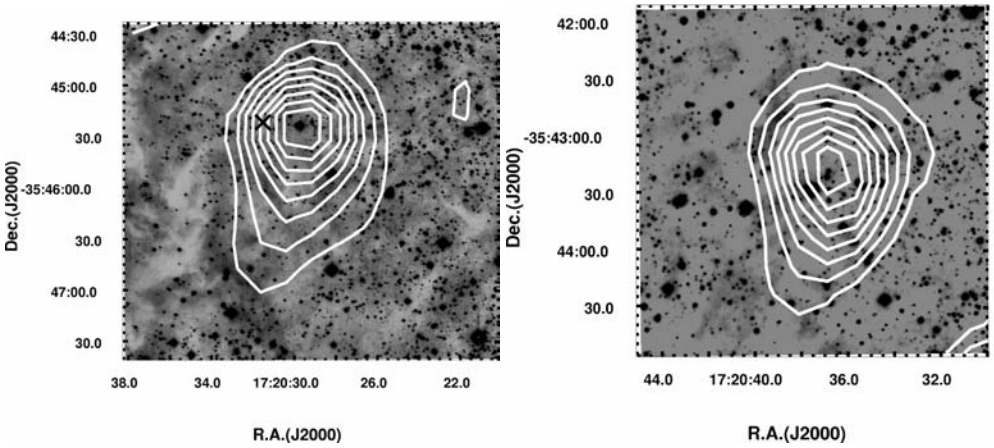

Figure 28. *Left*: K_s image of G351.39+0.73. The contours show the radio continuum emission at 1.4 GHz from NVSS). The cross indicates the position of IRAS $17171-3542$ *Right*: K_s image of G351.44+0.73 with the radio continuum emission at 1.4GHz (contours)

regions are part of the NGC 6334 complex molecular cloud. Fig. 28 shows K_s images obtained at Las Campanas with the 21 cm radio contours superposed.

G351.39+0.73 is associated with IRAS $17171-3542$. Roughly at the centre of the radio peak, a very red near-infrared source is found. Its near-infrared colours derived from 2MASS photometry are consistent with an early type star with $A_V = 20 - 30$. This source could be responsible for the ionization of the HII region.

Several near-infrared sources are present around the radio peak G351.44+0.73 (Fig. 28, right panel). The photometric analysis of this region, still in progress, should allow us to locate the infrared sources related to the radio continuum.

G351.02+0.65 This is the southernmost radio continuum source. The radio morphology of G351.02 +0.65 is shell-like with a large opening toward the southwest (see Fig. 5 of Carral et al. 2002). According to Carral et al. (2002) the nature of this object is still uncertain, although at the centre of the shell two O-type stars (HD 319703A (O7.5III(f): HD 319703B (O6.5Vf)) found by Walborn (1982) at the same distance of the complex (see Table 1) may be responsible for the ionization of G351.02+0.65.

5. Physical Parameters of the Active Centres of NGC 6334

The present work described in detail the observational results that have been published on the centres of star formation activity in the NGC 6334 complex. A summary of the derived properties of each of these is presented in Table. 3.

6. The Neighbouring Star Forming Region NGC 6357

The neighbouring large optical HII region NGC 6357 is located two degrees towards the Galactic Centre from NGC 6334 at a similar Galactic latitude (see Fig. 1 of Felli et al. 1990) and at a distance of 2.56 kpc (Massey et al. 2001). Its emission in visible

Table 3. Characteristics of the active subregions in NGC 6334

ID	α (J2000) h m s	δ ° ′ ″	Opt. (′)	Radio size (′)	Ioniz. stars	CO	Far-IR (′)	Near-IR size (″)	Ltot ($L_\odot$)	Masers	Age yr.
G351.02+0.65	17 19 45.6*	-36 05 06*	7	7	2 O7	no	?	7	?	no	10^6
V	17 19 57.6	-35 57 50	no	< 0.1	?	yes	1.4	-	$1.9\ 10^5$	H_2O, OH	10^5
G351.20+0.70	17 20 01.6*	-36 56 55*	no	2.2	B0	no	no	150	?	no	10^5
IV = A	17 20 19.0*	-35 54 50*	no	3	O7.5	yes	1.3	5 10	$2.2\ 10^5$	H_2O	10^5
G351.24+0.65	17 20 23.0	-36 55 24	no	< 1	?	no	< 1	5 - 10	?	no	$< 10^4$
G351.29+0.66	17 20 30.3$^+$	-35 52 49$^+$	0.2	< 1	?	no	30	?	?	no	?
III = C	17 20 32.0*	-35 51 26*	1.3	1.5	O8	yes	1	60	$1.8\ 10^5$	no	10^5
G351.39+0.73	17 20 29.6	-35 45 25	no	1.5	?	faint	> 8	50	$2.4\ 10^5$‡	no	?
G351.44+0.73	17 20 36.6	-35 43 20	no	< 1	?	no	no	2	$2.4\ 10^5$‡	no	?
II = D	17 20 44.5*	-35 49 25*	1.0	2.5	O6.5	yes	3.5	140	$2.6\ 10^5$	H_2O	10^6
G351.34+0.62	17 20 46.5†	-35 51 50†	0.8	< 1	?	yes	no	30	?	no	?
E	17 20 50.8*	-35 46 05*	no	0.5	O7.5	yes	< 1	40	$4.4\ 10^4$	no	10^4
I=F	17 20 53.6	-35 47 05	no	0.05	B0	yes	0.7	4	$1.5\ 10^5$	H_2O, CH_3OH, NH_3,OH	10^4
G351.20+0.47	17 20 56.8*	-36 04 05*	6	3	O7	no	no	2.5	?	no	10^6
I(N)	17 20 54.6	-35 45 09	no	no	?	yes	1.6	no	$4.9\ 10^4$	H_2O	$< 10^4$

NOTES: *: Extended source, coordinates of centre; $^+$: South of III; †: S of II; ‡: Combined luminosity of both sources

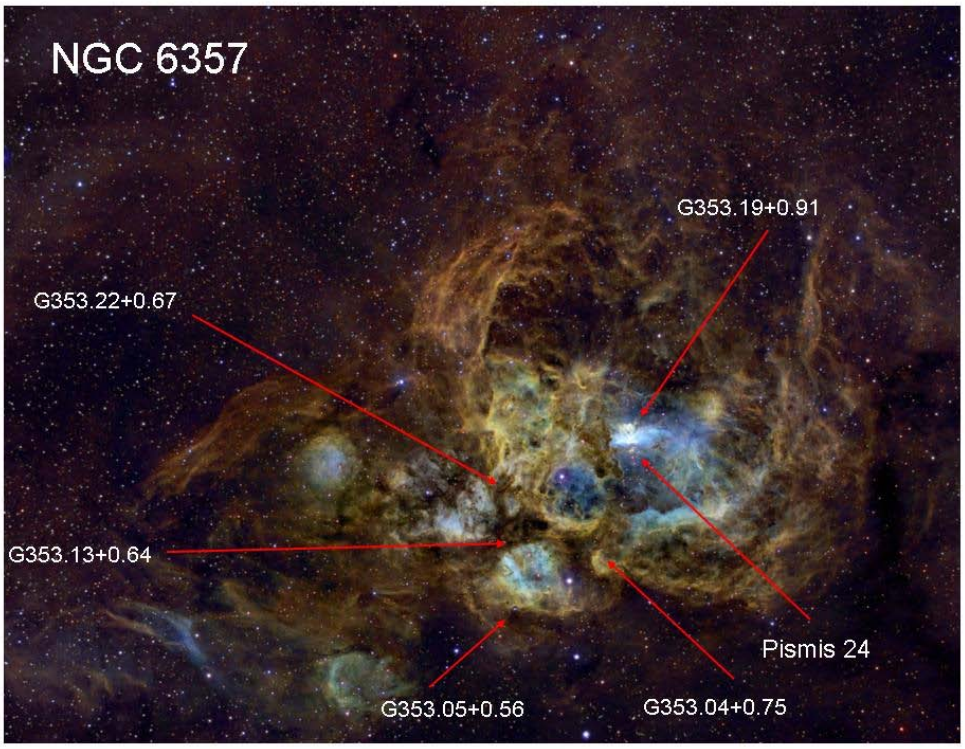

Figure 29. A wide field image of the NGC 6357 region. The field of view is approximately $1.7^o \times 1.3^o$. North is up, east is left. This is a composite [OIII] (blue), Hα (green) and [SII] (red) image, courtesy of Martin Pugh. The nucleus of the open cluster Pismis 24 is indicated. The position of the far-infrared peaks (McBreen et al. 1983) are labeled in Galactic coordinates. The scale is the same as in Fig. 30.

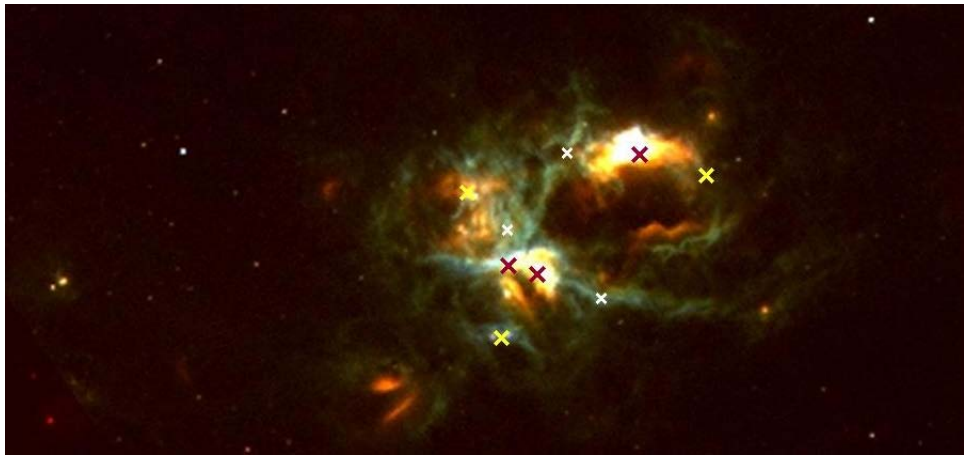

Figure 30. A composite *MSX* 8.3, 12.1 and 14.7 μm colour image of NGC 6357. The crosses mark the location of the *IRAS* 100 μm peaks. The sizes of the symbols indicate the relative brightness of the far-infrared emission. The scale is the same as in Fig. 29.

atomic lines, presented in Fig. 29, appears extremely filamentary with the presence of at least six shells or bubbles of ionized gas, each harbouring at least one central blue luminous star. This composite narrow-band photograph, taken in the lines [OIII] (blue), Hα (green) and [SII] (red) by Martin Pugh, shows a clear stratification of the high- and low-excitation lines as a function of the distance to those ionizing stars. In fact, some of these circular HII regions, like G353.1+10.6, resemble classical Strömgren spheres (Felli et al. 1990).

The most impressive of those cavities is the one created by the radiation and winds from the massive star cluster Pismis 24 (Pismis 1959), at a distance from the Sun of 2.56 kpc (Massey et al. 2001). At its nucleus, this cluster contains some of the most massive and luminous stars known: Pismis 24-1, a compact hierarchical triple system and the nearby single star Pismis 24-17. The mass of each of these four stars is nearly 100 $M_{\odot}$(Maíz-Apellániz et al. 2007). The rest of the hot O- and early B-type members of the cluster provide enough ionizing ($> 10^{50}$ UV photons s^{-1}, Bohigas et al. 2004) and kinetic energy to the surrounding expanding HII region. In particular to G353.19+0.91, the brightest radio far-infrared and visible HII region ($L_{\rm IR} \simeq 6\ 10^5 L_{\odot}$, McBreen, Jeffe & Fazio 1983; $M_{\rm gas} \simeq 100 M_{\odot}$, Bohigas et al. 2004). This peculiar-looking nebula, with a conspicuous elephant trunk pointing straight into the nucleus of Pismis 24, is located only one arcminute (0.7 pc) to the north of the hottest stars.

Several young stellar objects embedded in G353.19+0.91 have been detected in the near-infrared by Persi et al. (1986), Felli et al. (1990), Bohigas et al. (2004) and in X-rays by Wang et al. (2007). These have been found to contribute locally to the ionization and heating of their surrounding gas and dust environment (Felli et al. 1990).

Other bright radio-continuum (Schraml & Mezger 1969) and far-infrared peaks with $L_{\rm IR} > 10^5 L_{\odot}$(McBreen et al. 1983) are located in regions of high obscuration, close to boundaries of optically visible HII regions (Figs. 29 and 30). The radio HII region and far-infrared source G353.13+0.64 has been studied by Persi et al. (1986) and Felli et al. (2000). It also contains young embedded stars that heat the surrounding dust in a dense CO clump. Its location, at the edge of the developed HII region G353.1+10.6, suggests that its recent star formation phase was triggered by the interaction of the expanding HII region with the high-density molecular clump.

Acknowledgments. We thank Martin Pugh for the use of Figures 1 and 29. We made use of archived data products from the *Midcourse Space Experiment*. Processing of its data was funded by the Ballistic Missile Defense Organization with additional support from NASA Office of Space Science. We also made use of 2MASS data of the NASA/ IPAC Infrared Science Archive, which is operated by the Jet Propulsion Laboratory, California Institute of Technology, under contract with the National Aeronautics and Space Administration and of GLIMPSE data obtained with IRAC on the *Spitzer Space Telescope*, which is operated by the Jet Propulsion Laboratory, California Institute of Technology, under NASA contract 1407. Part of this work was supported by DGAPA/UNAM project IN102803. It is a pleasure to acknowledge the participation in the WIRC and other near-infrared surveys mentioned in this review of our collaborator, Miguel Roth. We also thank Göran Sandell and Bo Reipurth for carefully reading the manuscript and providing suggestions that improved the content of this review. NGC 6334 and NGC 6357 are included in a Herschel Guaranteed Time Key Program "Herschel imaging survey of OB young stellar objects" (HOBYS).

References

Alvarez, C., Feldt,M., Henning,T., Puga, E., Brandner, W., & Stecklum, B. 2004, ApJS, 155, 123
Argon, A. L., Reid, M. J., & Menten, K. M. 2000, ApJS, 129, 159
Bachiller, R. & Cernicharo, J. 1990, A&A, 239, 276
Bassani, L., De Rosa, A., Bazzano, A., et al. 2005, ApJ, 634, L21
Benjamin, R. A., Churchwell, E., Babler, E. L., et al. 2003, PASP, 115, 953
Beuther, H., Thorwirth, S., Zhang, Q., Hunter, T. R., Megeath, S. T., Walsh, A. J., & Menten, K. M. 2005, ApJ, 627, 834
Beuther, H., Walsh, A. J., Thorwirth, S., Zhang, Q., Hunter, T. R., Megeath, S. T., & Menten, K. M. 2007, ApJ, 466, 989
Beuther, H., Walsh, A. J., Thorwirth, S., Zhang, Q., Hunter, T. R., Megeath, S. T., & Menten, K. M. 2008, A&A, 481, 169
Bohigas, J. 1992, RevMex, 24, 121
Bohigas, J., Tapia, M., Roth, M., & Ruíz, M. T. 2004, AJ, 127, 2826
Bok, B. J., Bester, M. J., & Wade, C. M. 1955, Daedalus 86, 9 (Harvard Repr. 416)
Boreiko, R. T. & Betz, A. L. 1995, ApJ, 454, 307
Braz, M. A. & Epchtein, N. 1983, A&AS, 54, 167
Brooks, K. J. & Whiteoak, J. B. 2001, MNRAS, 320, 465
Burton, M. G., Ashley, M.C.B., Marks, P.D., et al. 2000, ApJ, 542, 359
Bykov, A.M., Krassilchtchikov, A.M., Uvarov, Y.A., et al. 2006, A&A, 449, 917
Caproni, A., Abraham, Z., & Vilas-Boas, J. W. S. 2000, A&A, 361, 385
Carral, P., Kurtz, S. E., Rodríguez, L. F., De Pree, C., & Hofner, P. 1997, ApJ, 486, L103
Carral, P., Kurtz, S. E., Rodríguez, L. F., Menten, K., Cantó, J., & Arceo, R. 2002, AJ, 123, 2574
Cheung, L., Frogel, J. A., Hauser, M. G., & Gezari, D. Y. 1978, ApJ, 226, L149
Chrysostomou, A., Hough, J.H., Aspin, C., & Bailey, J.A. 1994, MNRAS, 268, L63
Condon, J.J., Cotton, W. D., Greisen, E. W., et al. 1998, AJ, 115, 1693
Conti, P. S. 1988, in *O stars and Wolf-Rayet stars*, ed. P. S. Conti & A. H. Underhill (Washington, D.C.: NASA SP-497), p. 119
Davis, C. J. & Eislöffel J. 1995, A&A, 300, 851
De Buizer, J.M., Piña, R.K., & Telesco, C. M. 2000, ApJS, 130, 437
De Buizer, J.M., Radomski, J.T., Piña, R.K., & Telesco, C. M. 2002, ApJ, 580, 305
De Pree, C. G., Rodríguez, L. F., Dickel, H. R., & Goss, W. M. 1995, ApJ, 447, 220
Deharveng, L., Lefloch, B., Zavagno, A., et al. 2003, A&A, 408, L25
Dickel, H. R., Dickel, J. R., & Wilson, W. J. 1977, ApJ, 217, 56
Dreyer, J. L. E. 1888, Mem. Royal Astron. Soc. 49, Part I, 1
Ellingsen, S. P., Norris, R. P., & McCulloch, P. M. 1996, MNRAS, 279, 101
Emerson, J.P., Jennings, J.B., & Moorwood, A.F.M. 1973, ApJ, 184, 401
Ezoe, Y., Kokubun, M., Makishima, K., Sekimoto, Y, & Matsuzaki, K. 2006, ApJ, 638, 860
Felli, M., Persi, P., Roth, M., Tapia, M., Ferrari-Toniolo, M., & Cervelli, A. 1990, A&A, 232, 477
Fischer, J., Joyce, R. R., Simon, M., & Simon, T. 1982, ApJ, 258, 165
Forster, J. R. 1993, in *Astrophysical Masers*, ed. A. Clegg & G. Nedoluha (Berlin: Springer), 108
Forster, J. R. & Caswell, J. L. 1989, A&A, 213, 339
Gardner, F. F. & Whiteoak, J.B. 1975, MNRAS, 173, 131
Gaume, R. A. & Mutel, R. L. 1987, ApJS, 65, 193
Georgelin, Y.P. & Georgelin, Y.M. 1970, A&A, 6, 349
Gezari, D. Y. 1982, ApJ, 259, L29
Goss, W. M. & Shaver, P. A. 1970, Austr. J. Phys. Ap. Suppl, No. 14, 1
Gum, C. S. 1955, Mem. Royal Astron. Soc., 67, 155
Gyulbudaghian, A.L., Glushkov, Yu, I., & Denisyuk, E. 1978, ApJ, 224, L37

Harris, D., Maccacaro, T., Forman, W., et al. 1990, in *The Einstein Observatory Catalogue of IPC X-Ray Sources*, (Cambridge: Smithsonian Astrophysical Observatory)
Harvey, P. M. & Gatley, L. 1983, ApJ, 269, 613
Harvey, P. M. & Wilking, B.A. 1984, ApJ, 280, L19
Harvey, P. M., Hyland, A. R., & Straw, S. M. 1987, ApJ, 317, 173
Hase, G. A. & Shajn, E. V. 1955, Bull. Crimea Ast. Obs., 15, 11
Hashimoto, J., Tamura, M, Suto, H., Abe, L., Ishii, M., Kudo, T., & Mayama, S. 2007, PASJ, 59, 221
Hashimoto, J., Tamura, M., Kandori, R., Kusakabe, N., Nakajima, Y., Kurita, M., Nagata, T., Nagayama, T, Hough, J., & Chrysostomou, A. 2008, ApJ, 677, L39
Herschel, J. 1864, Philosophical Transactions Royal Society, 154, 1
Hunter, T. R., Brogan, C. L., Megeath, S. T., Menten, K. M., Beuther, H., & Thorwirth, S. 2006, ApJ, 649, 888
Jackson, J. M. & Kraemer, K. E. 1999, ApJ, 512, 260
Johnson, H. L. 1966, ARAA, 4, 193
Kim, S. & Narayanan, D. 2006, PASJ, 58, 753
Kogan, L. & Slysh, V 1998, ApJ, 497, 800
Koornneef, J. 1983, A&A, 128, 84
Kraemer, K. E. 1998, Ph.D. thesis, Boston Univ.
Kraemer, K. E. & Jackson, J. M. 1995, ApJ, 439, L9
Kraemer, K. E. & Jackson, J. M. 1999, ApJS, 124, 439
Kraemer, K. E., Jackson, J. M., Paglione, T.A.D., & Bolatto, A.D. 1997, ApJ, 478, 614
Kraemer, K. E., Jackson, J. M., & Lane, A. P. 2000, ApJ, 503, 785
Kraemer, K. E., Deutsch, L. K., Jackson, J. M., Hora, J. L., Fazio, G. G., Hoffmann, W. F., & Dayal, A. 1999, ApJ, 516, 817
Kraemer, K. E., Jackson, J. M., Lane, A. P., & Paglione, T. A. D. 2000, ApJ, 542, 946
Kuiper, T.B.H., Peters, W.L., Forster, J.R., Gardner, F.F., & Whiteoak, J.B. 1995, ApJ, 446, 692
Leurini, S, Schilke, P., Parise, B., Wyrowski, F. Güsten, R., & Philipp, S. 2006, A&A, 454, L83
Loughran, L., McBreen, B., Fazio, G. G., Rengarajan, T. N., Maxson, C. W., Serio, S., Sciortino, S., & Ray, T. P. 1986, ApJ, 303, 629
Maíz-Apellániz, J., Walborn, N. R., Morrell, N. I., Niemela, V. S., & Nelan, E. P. 2007, ApJ, 660, 1480
Massey, P., DeGioia-Eastwood, K., & Waterhouse, E. 2001, AJ, 121, 1050
McBreen, B., Fazio, G. G., Stier, M., & Wright, E. L. 1979, ApJ, 232, L183
McBreen, B., Jaffe, D. T. & Fazio, G. G. 1983, AJ, 88, 835
McCutcheon, W. H., Sandell, G., Matthews, H. E., Kuiper, T. B. H., Sutton, E. C., Danchi, W. C., & Sato, T. 2000, MNRAS, 316, 152
Megeath, S. T. & Tieftrunk, A. R. 1999, ApJ, 526, L113
Menten, K. M. & Batrla, W. 1989, ApJ, 341, 839
Migenes, V., Horiuchi, S, Slysh, V.I., et al. 1999, ApJS, 123, 478
Miettinen, O., Harju, J., Haikala, K., & Pomrèn, C. 2006, A&A, 460, 721
Moorwood, A. F. M. & Salinari, P. 1981, A&A, 102, 197
Moran, J. M. & Rodríguez, L. F. 1980, ApJ, 236, L159
Moran, J. M., Rodríguez, L. F., Greene, B., & Backer, D. C. 1990, ApJ, 348, 147
Muñoz, D.J., Mardones, D., Garay, G, Rebolledo, D., Brookes, K., & Bontemps, S. 2007, ApJ, 668, 906
Nakagawa, T, Nagata, T., Matsuhara, H, Okuda, H., Shibai, H., & Hayashi, S.S. 1990, ApJ, 351, 573
Neckel, T. 1978, A&A, 69, 51
Neckel, T. & Chini, R. 1981, A&AS, 45, 451
Norris, R. P., Whiteoak, J. B., Caswell, J.L., Wieringa, M. H., & Gough, R. G. 1993, ApJ, 412, 222
Norris, R. P., Byleveld, S. E., Diamond, P. J., et al. 1998, A&A, 508, 275
Persi, P. & Ferrari-Toniolo, M. 1982, A&A, 112, 292
Persi, P., Ferrari-Toniolo, M., Roth, M., & Tapia, M. 1986, A&A, 170, 97

Persi, P., Roth, M., Tapia, M., Marenzi, A. R., Felli, M., Testi, L., & Ferrari-Toniolo, M. 1996, A&A, 307, 591
Persi, P., Tapia, M., Felli, M., Lagage, P.,O., & Ferrari-Toniolo, M. 1998, A&A, 336, 1024
Persi, P., Tapia, M., & Roth, M. 2000, A&A, 357, 1020
Persi P., Tapia M., Roth M., Gomez M., & Marenzi A.R. 2005a, in *The Dusty and Molecular Universe. A prelude to Herschel and ALMA*, ESA SP-577, p.407
Persi P., Tapia M., Roth M., Gomez M., & Marenzi A.R. 2005b, in *Massive Star Birth: A Crossroads of Astrophysics*, Proc. IAU Symposium No. 227, ed. R. Cesaroni, M. Felli, E. Churchwell, & M. Walmsley, (Cambridge: Cambridge University Press), p. 291
Persi P. & Marenzi A.R. 2006, Chinese Journal of A&A, 6, 125
Persi, P., Tapia, M., Roth, M., & Gómez, M. 2008, submitted to A&A
Pismis, P. 1959, Bol. Obs. Tonantzintla Tacubaya, 2, 37
Poveda, A. 1977, Rev. Mex. Astron. Astrofis., 3, 189
Rengarajan, T. N. & Ho, P. T. P. 1996, ApJ, 465, 363
Rodgers, A. W., Campbell, C.T., & Whiteoak, J.B. 1960, MNRAS, 121, 103
Rodríguez, L. F., Cantó, J., & Moran, J. M. 1982, ApJ, 255, 103
Rodríguez, L. F., Cantó, J., & Moran, J. M. 1988, ApJ, 333, 801
Rodríguez, L. F., Zapata, L.A., & Ho, P.T.P. 2007, ApJ, 654, L143
Roslund, C., 1966, Arkiv Ast., 4, 101
Sandell, G. 1999, A&A, 343, 281
Sandell, G. 2000, A&A, 358, 242
Sarma, A. P., Troland, T. H., Roberts, D. A., & Crutcher, R. M. 2000, ApJ, 533, 271
Schilke, P., Comito, C., Thorwirth, S., et al. 2006, A&A, 454, L41
Schraml, J. & Mezger, P. G. 1969, ApJ, 156, 269
Schwartz, P. R., Snell, R. L., & Schloerb, F. P. 1989, ApJ, 336, 519
Sekimoto, Y., Matsuzaki, K., Kamae, T., Tatematsu, K., Yamamoto, S., & Umemoto, T. 2000, PASJ, 52, L31
Sharpless, S. 1953, ApJ, 118, 362
Sharpless, S. 1959, ApJS, 4, 257
Simon, T., Dyck, H. M., Wolstencroft, R. D., McLean, I. S., Joyce, R. R., & Johnson, P. E. 1985, MNRAS, 212, 21P
Skrutskie, M. F., Cutri, R. M., Stiening, M., et al. 2006, AJ, 131, 1063
Straw, S. M. & Hyland, A. R. 1989a, ApJ, 340, 318
Straw, S. M. & Hyland, A. R. 1989b, ApJ, 342, 876
Straw, S. M., Hyland, A. R., & McGregor, P. J. 1989, ApJS, 69, 99
Tapia, M., Roth, M., Marraco, H., & Ruiz, M. T., 1988, MNRAS, 232, 661
Tapia, M., Persi, P., & Roth, M. 1996, A&A, 316, 102
Thorwirth, S., Winnewisser, G., Megeath, S.T., & Tieftrunk, A.R. 2003, in ASP Conf. Ser. 287, *Galactic Star Formation Across the Stellar Mass Spectrum*, ed. J.M. De Buizer & N.S. van der Bliek (San Francisco: ASP), 257
Townsley, L. K., Feigelson, E. D., Montmerle, T., et al. 2003, ApJ, 593, 874
Wilson, R. W. & Bolton, J. G. 1960, PASP, 72, 331
Walborn, N. R. 1982, AJ, 87, 1300
Walsh, A. J., Burton, M. G., Hyland, A. R., & Robinson, G. 1998, MNRAS, 301, 640
Wang, J., Townsley, L. K., Feigelson, E. D., Getman, K. V., Broos, P. S., Garmire, G. P., & Tsujimoto, M. 2007, ApJS, 168, 100
Wolstencroft, R. D., Scarrott, S. M., & Warren-Smith, R. F. 1987, MNRAS, 228, 805
Zhang, J.S., Henkel, C., Mauersberger, R., Chin, Y.-N., Menten, K.M., Tieftrunk, A.R., & Belloche, A. 2007, A&A, 465, 887